Review

Silver and Gold Containing Compounds of p-Block Elements As Perspective Materials for UV Plasmonics

Rosen Todorov, Temenuga Hristova-Vasileva,* Vesela Katrova, and Anna Atanasova

Cite This: *ACS Omega* 2023, 8, 14321−14341

Read Online

ACCESS | Metrics & More | Article Recommendations

ABSTRACT: We present a review of phase formation tendencies, methods for preparation and optical properties of alloys and compounds from the binary systems of silver or gold with metals and metalloids from the p-block of the Periodic system of elements. Reference data about the homogeneity regions in the systems of interest, together with information about the crystalline structure of existing indexed compounds in them, is proposed and statistically analyzed. General background for the synthesis of intermetallic alloys and compounds, and the tendencies for their preparation for plasmonic purposes are presented. The high plasma frequency, ω_p of p-block metals makes their alloys with silver and gold an interesting object of study, due to the possibility of ω_p variation over a wide interval in the ultraviolet (UV) spectral region with a view to finding more efficient materials for excitation of a localized surface plasmon resonance (LSPR) necessary for various applications and techniques operating in this part of the electromagnetic spectrum. Unlike the alloys between the noble metals Cu, Ag, and Au, which form continuous series of solid solutions, different areas can be observed in the phase diagrams of the Ag(Au)−p-block systems, containing solid solutions, intermetallic compounds, and heterogeneous mixtures. The ability to vary the plasma frequency of solid solutions, like the alloys between the noble metals Cu, Ag, and Au, is the reason to pay attention to the compositions of the Ag(Au−p-block systems that fall in these regions of their phase diagrams. The analysis of the published results for complex permittivity shows that the addition of small amounts of conductive p-block elements to noble metals reduces the energy gap for interband transitions and increases their plasmonic activity in the UV spectral range. The article analyzes the relationship between electrical resistivity and LSPR excitation efficiency, which shows that the intermetallic compounds from Ag(Au)−p-block systems with a well-ordered crystalline structure and good conductivity level can be more effective materials for UV plasmonics than the boundary solid solutions. Intermetallic compounds can be easily obtained in the form of bulk samples, thin films, and nanoparticles with controlled size and geometric shape. The spectral dependences of the plasmon efficiency of the intermetallic compounds, determined from their complex permittivity functions, show that they are promising materials for excitation of LSPR in the UV spectral region.
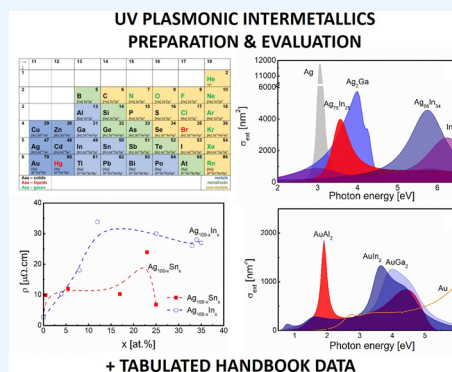
1. INTRODUCTION

The rapid vibrations of the electron gas in conducting media, such as metals, are called plasma oscillations, and their frequency is determined by the type of material. At the plasma frequency, the propagation vector vanishes, so the electrons in the metal must interact collectively to ban the electromagnetic wave from the interior of the material. The phenomenon when plasma oscillations propagate along a metal surface excited by electromagnetic (EM) radiation is called surface plasmon resonance (SPR).[1] Plasmonics is the study of these particular light-matter interactions, which have enabled a vast array of applications, including surface-enhanced spectroscopies,[2] biological and chemical sensing,[3] and lithographic fabrication.[4] In the case when the light interacts with plasmonic waves, which propagate on the surface of metallic particles much smaller than the incident wavelength, a localized surface plasmon resonance (LSPR) is observed. The LSPR strongly enhances the incident EM field near the nanostructure. One of the main

tasks of nanophotonics is to model and study how the size and shape of metal nanoparticles interact with light. As a result of this analysis, the LSPR makes possible the light trapping in solar cells,[5] achieving of ultrahigh sensitivity of sensing methods based on phenomena such as surface-enhanced Raman scattering and surface-enhanced luminescence,[6] application of metallic nanoparticles as biosensors.[7]

To support SPR or LSPR, the materials must possess a negative real and small positive imaginary dielectric constant. This is the reason why different materials are effective for

exciting SPR or LSPR in a certain spectral interval of the EM spectrum.[1] The low optical losses of silver in the visible and near-infrared spectral regions are the reason it to be the most effective material for exciting an SPR in the visible spectral region.[8] Although less efficient than silver, the chemical stability of gold is the reason why it finds application as a plasmonic material in almost the same spectral range. Unfortunately, an increase in the losses of these two metals in the infrared spectral region leads to decrease of their efficiency. Therefore, oxides and nitrides of transition metals are used as plasmonic materials in this part of the electromagnetic spectrum.[9,10]

The energy of photons in the UV spectral region is greater than that of the photons in visible light. This is the reason for the observation of a number of light phenomena inherent to this region of the electromagnetic spectrum. UV light finds application in a number of fields such as spectroscopy, imaging, microscopy, quantum optics, lithography, light therapy, micromachining, and sterilization.[11] The strong absorption of the UV light by conventional optics and the low-efficiency of photodetectors may be the reason for the reduction in the efficiency of the applications and techniques mentioned above. The usage of surface plasmon phenomena in the UV spectral region can significantly improve quantum yields and increase the sensitivity of the different surface-enhancement spectroscopic methods, as well as the emission of light-emitting diodes.[11] In addition, the bond energy of most materials is commensurate with the photon energy in the UV spectral region, photodissociation, ionization, and photoisomerization. Consequently, the use of phenomena such as LSPR and plasmonic antenna effect increases the catalyst's ability to absorb light, thereby increasing its efficiency in photocatalyst reactions.[12]

While there are a number of materials effective for SPR excitation in the visible and infrared spectral regions, the search for effective plasmonic materials in the ultraviolet (UV) region is still an up-to-date task.[13] The presence of interband transitions with photon energies that fall into the ultraviolet are the reason why silver and gold have low efficiency for excitation of surface plasmon resonance in this region of the electromagnetic spectrum. The higher plasma frequency of p-block metals, such as Al, Ga, and In, compared to that of noble metals is the reason why they are found suitable for excitation of LSPR in the UV spectral region.[13,14]

2. OPTICAL PROPERTIES OF NOBLE METALS AND ALLOYS BETWEEN THEM

The metallic alloys are expanding the list of possible plasmonic materials, as they offer a potential for tuning the optical and physical properties of pure metals for optimal performance.[15] The lower efficiency of localized surface plasmon resonance (LSPR) properties of gold nanocrystals can be further improved through alloying with silver.[15] As silver and gold are the main materials used for plasmonics in the visible spectral region, before considering the properties of their alloys with the p-block metals, we will briefly discuss the optical properties of the noble metals and some of their alloys with alkali elements and transition metals. Theory of the optical properties and band structure of noble metals can be found in the paper of Simmons et al.[16] The properties of the noble metals of group 11 of the Periodic table of chemical elements, Cu, Ag, and Au, are determined by their electronic structure (Figure 1). As elements belonging to the same group, they

Figure 1. Excerpt of the Periodic table of elements: p-block + groups 11 and 12 (Cu, Ag, Au, Zn, Cd, and Hg), with their electronic structures, states of matter, and conductivity properties.

have a similar electronic structure (Cu, $[Ar]3d^{10}4s^1$; Ag, $[Kr]4d^{10}5s^1$; and Au, $[Xe]4f^{14}5d^{10}6s^1$). Their complex permittivity is $\varepsilon = \varepsilon' + i \cdot \varepsilon''$ consists of contributions from the free s electrons and bound electrons of the d electronic level. The contribution of free electrons of silver on the real part of the dielectric function changes its sign at 9.2 eV (free electron plasmon frequency, ω_p), as the 4d electrons are bound and their contribution to the dielectric constant is at 4.0 eV. It is large enough for the real part of complex permittivity to overcome zero and places the plasmon frequency close to 3.9 eV.[17] To distinguish it from the free electron plasmon frequency, this frequency is often called screen plasmon frequency, ω_s.

A similar behavior is observed in two other elements from the same group, copper and gold.[16] In the case of copper, the 3d electrons are bound and only the 4s electrons can be continuously excited. The top of the filled 3d band occurs at 2.2 eV below the Fermi level in the 4s band. Consequently, the 3d bound electrons can be excited with photons of energy equal to or greater than 2.2 eV. Since the 3d electrons of copper are closer to the nucleus of the atom and therefore more strongly bound, their contribution to the total complex permittivity is weaker and it remains negative in the spectral interval between 2.2 and 7.2 eV. The energy difference between the filled d band and the Fermi energy for Au is 2.5 eV. This is the reason for the yellow color of gold.

Since Cu, Ag, and Au have the same crystalline lattice, they have the ability to form continuous series of solid solutions between them. By varying the composition of bimetallic noble metal alloys, it becomes possible to tune the plasmon frequency and improve the efficiency of the localized surface plasmon resonance.[15,18] It has been shown by Peña-Rodríguez[19] that the Drude-Lorentz model gives a good description of the dielectric function of Ag−Au alloys. It was found that the plasmon frequency, ω_p in the Drude part, as well as the frequencies related with interband transitions in the Lorenzian part, ω_i, follow a linear dependence, while the damping parameter Γ is in a quadratic dependence. According to the authors, the compositional dependence of Γ is determined by two factors: (1) the electrical resistivity is usually larger for the alloys, due to the introduction of additional impurities that produce an increase in the number of different scattering mechanisms and (2) the additional contribution may be explained by the differences in electronegativity between gold and silver, which supports consid-

Table 1. Summary of Literature Data on Optical Properties (Reflectivity, R, Refractive Index, n, Extinction Coefficient, k, and Complex Permittivity, ε) and Plasmonic Properties (Drude Plasmon Frequency, ω_p, Screening Plasmon Frequency or the Crossover Point of Real Part of Complex Permittivity ($\varepsilon' = 0$), ω_s, Coefficient of Efficiency for LSPR Excitation, Q_{LSPR}, and Cross-Section of Extinction, σ_{ext}) of Intermetallic Alloys of (a) Noble Metals Silver and Gold and (b) p-Block Elements[a]

material	sample	available optical data and spectral range	ω_p (eV)	ω_s (eV)	$Q_{LSPR}/\omega(Q_{LSPR})$ (eV)	$\sigma_{ext}/\omega(\sigma_{ext})$ (eV)	ref
Ag	TF	ε (0.4–10 eV)	9.219	3.9	~100/2.0 eV	n.a.	20
Ag	n.a.	n.a.	9.015	n.a.	n.a.	n.a.	15
Au	TF	ε (0.4–10 eV)	9.103	2.25	53.6/1.5 eV	n.a.	20
Au	TF	n.a.	8.769	n.a.	n.a.	n.a.	15
Ag-Au	TF	ε (0.7–6.2 eV)	8.893 for Au48Ag52 TF	~3.75 eV for Ag90Au10 and Ag74Au26 TF's 6.0 eV for Ag10Au90 TF $\varepsilon' < 0$ in this spectral interval for Ag50Au50 TF	~12/1.7 eV[d] for Ag90Au10 TF's	n.a.	15
Ag-Cu	TF	ε (0.7–6.2 eV)	n.a.	~4.0 eV for Ag90Cu10 TF for thin films with higher Cu content $\varepsilon' < 0$ in this spectral interval	~6/1.35 eV[d] for Ag90Cu10 TF's	n.a.	15
Au-Cu	TF	ε (0.7–6.2 eV)	n.a.	~3.54 eV for Ag90Cu10 TF for thin films with higher Cu content $\varepsilon' < 0$ in this spectral interval	~4/1.40 eV[d] for Ag90Cu10 TF's	n.a.	15
Ag-Co	TF	n.a.	n.a.	n.a.	n.a.	1.2–1.65 eV	23
alkali–noble intermetallic compounds							
material	sample	available optical data and spectral range	ω_p (eV)	ω_s (eV)	$Q_{LSPR}/\omega(Q_{LSPR})$ (eV)	$\sigma_{ext}/\omega(\sigma_{ext})$ (eV)	ref
LiAg	DFT	ε (0.4–10 eV)	7.28	4.72	5.97/0.569 eV	n.a.	20
LiAu	DFT	ε (0.4–10 eV)	7.20	4.44	6.33/0.686	n.a.	20
NaAg	DFT	ε (0.4–10 eV)	6.47	0.80	3.16/0.928	n.a.	20
NaAu	DFT	ε (0.4–10 eV)	4.84	1.08	6.25/0.761	n.a.	20
KAg	DFT	ε (0.4–10 eV)	3.10	0.97	2.470.541	n.a.	20
KAu	DFT	ε (0.4–10 eV)	1.54	0.52	7.32/0.297	n.a.	20
p-block elements							
chemical element	sample	available optical data and spectral range	ω_p (eV)	ω_s (eV)	$Q_{LSPR}/\omega(Q_{LSPR})$ (eV)	$\sigma_{ext}(nm^2)/\omega(\sigma_{ext})$ (eV)	ref
Zn	B	n.a.	n.a.	n.a.	3.59/3.60[c]	n.a.	31
Cd	B	n.a.	n.a.	n.a.	3.63/0.65[c]	n.a.	31
Al	B	n.a.	n.a.	n.a.	9.3/8.6[b]	~6230/6.0[b]	13
Al	DFT	n.a.	n.a.	n.a.	13.58/11.0[c]	n.a.	31
Ga	TF	ε (0.5–11.6 eV)	14.344[b]	n.a.	n.a.	~2900/6.2[b]	13
Ga	–	ε (0.124–10000 eV)	9.954[b]	n.a.	n.a.	n.a.	32
Ga	TF	R, n, k, ε (2–15 eV)	14.05	14.05	n.a.	n.a.	33
Ga	DFT	n.a.	n.a.	n.a.	3.41/8.30[c]	n.a.	31
Ga	TF	ε (1.9–3 eV)	n.a.	$\varepsilon' < 0$ in investigated spectral range	n.a.	n.a.	34
In	NPs	1.5–6 eV	n.a.	n.a.	tunable localized surface plasmon resonances in spectral range 3.5–6 Ev	n.a.	26
In	–	n, k (0.12–10000 eV)	n.a.	~11.7	n.a.	~7470/10.5[b]	32
In	B	ε (0.5–11.6 eV)	10.936[b]	n.a.	n.a.	n.a.	13
In	—	n.a.	n.a.	n.a.	4.60/5.10[c]	n.a.	31
In	TF	ε (0.6–6.5 eV)	n.a.	n.a.	n.a.	~3000/6.2	35
In	TF	n, k (1.9–3 eV)	n.a.	$\varepsilon' < 0$ in investigated spectral range	n.a.	n.a.	34

Table 1. continued

			p-block elements				
chemical element	sample	available optical data and spectral range	ω_p (eV)	ω_s (eV)	$Q_{LSPR}/\omega(Q_{LSPR})$ (eV)	$\sigma_{ext}(nm^2)/\omega(\sigma_{ext})$ (eV)	ref
Tl	B	ε (1.5–12 eV)[b]	6.314[b]	n.a.	n.a.	~1280/5.89[b]	13
	DFT	n.a.	n.a.	n.a.	2.71/3.20[c]	n.a.	31
	TF	ε (1.9–3 eV)	n.a.	$\varepsilon' < 0$ in investigated spectral range	n.a.	n.a.	34
Sn	–	n, k (0.1–10000 eV)	n.a.	~13.8	n.a.	n.a.	32
	B	n.a.	12.439[b]	n.a.	n.a.	~2000/5.30	13
	DFT	n.a.	n.a.	n.a.	3.50/2.25[c]	n.a.	31
	TF	ε (0.6–6.5 eV)	7.33–9.72 eV for thin films obtained at different deposition rates	n.a.	n.a.	n.a.	29
Pb	B	ε (1.5–12 eV)[b]	9.210[b]	n.a.	n.a.	~1960/5.8	13
	DFT	n.a.	n.a.	n.a.	3.07/5.95[c]	n.a.	31
	–	n, k (1–10000 eV)	n.a.	~12.7	n.a.	n.a.	32
Sb	DFT	n.a.	n.a.	n.a.	1.33/3.50[c]	n.a.	31
	B	n.a.	n.a.	~0.4	n.a.	n.a.	28
Bi	B	ε (1.5–12 eV)[b]	9.004[b]	n.a.	n.a.	~910/4.3	13
	DFT	n.a.	n.a.	n.a.	2.71/3.07[c]	n.a.	31
	–	ε (0.124–3.1 eV)	n.a.	n.a.	n.a.	n.a.	32
	B	R, ε (0.01–0.08 eV)	~0.1	n.a.	n.a.	n.a.	36

[a] B, bulk; TF, thin film; DFT, density functional theory (DFT) calculation; Q_{LSPR}, coefficient of efficiency for LSPR excitation (see section 5); and σ_{ext}, cross-section extinction (see section 6). [b] For the ε and ω_p data presented in ref 13, data used from the authors of ref 31 to calculate the Q_{LSPR}, see the list of references cited in the paper. [c] For the data used in ref 31 to calculate the Q_{LSPR}, see the list of references cited in the paper. [d] Published data in ref 15 was used to calculate Q_{LSPR} and $\omega(Q_{LSPR})$.

erable transfer of electronic density from Ag to Au. These conclusions show the possibility to model and select a composition of Ag−Au alloy with desired properties.

The ability to vary the plasmonic properties by making alloys with different plasma frequencies is the reason to model and study different alloys of gold and silver. The optical properties and plasmonic activity of alkali−noble metal alloys are modeled and reviewed in reference 20. The alloying of alkali metal in silver and gold results in a shift of both the free electron plasmon frequency and also the screening plasmon frequency in the infrared spectral region. Other interesting groups of alloys of silver is this with transition metals, such as Co and Ni. These alloys are promising from the point of view of their magnetic properties and the possibility to observe a magnetoplasmonic effect.[21−23]

The so-called p-block of the Periodic system of elements consists of materials with valence electrons in the upper p-orbital of their electronic configuration. The p-block elements (Figure 1) can be divided into three subgroups, according to their properties, metals, metalloids, and nonmetals, including the groups of halogens and noble gases. As the subject of our review are the solids with plasmonic activity, we will not discuss the mixtures of silver and gold with the noble gases group, due to their volatility, and with the nonmetals, since they are not conductive enough. In addition to the p-block elements, we will also analyze the silver and gold containing phases of the elements Cd, Zn, and Hg (Figure 1), which have a fully filled s-atomic orbital in their ground state, and a relativistic effect could be expected in them due to their filled d-electrons layer.

It is known that the plasmon frequency of the p-block metals lie in the deep UV spectral region.[13,14,24−26] The presence of interband transitions in the infrared and visible spectral region[27−29] leads to a decrease in their efficiency for excitation of LSPR in the IR spectral region and a better efficiency in the UV spectral region compared to silver and gold. These characteristics of the p-block metals are a reason to study their alloys with the noble metals, because a tuning of plasmon frequency with enough efficiency in the UV spectral region is expected to be achieved.[30,31]

Table 1 summarizes results on optical and plasmonic properties of elements and alloys of noble metals and p-block metals, derived from both physical samples (thin films and bulks) and from theoretical calculations (DFT functions). Due to the large number of sources for Si and Ge,[32] the information about them was not included in the table. It can be seen that in most cases the p-block elements have a higher plasmonic frequency, as well as demonstrate better efficiency at higher photon energies falling into the UV spectral region.

3. PHASE EQUILIBRIA IN SILVER/GOLD−P-BLOCK METAL SYSTEMS

The best case for fluent tuning of a given property by addition of a second element (doping or alloying) is when the two elements or compounds fully dissolve in each other by forming continuous rows of solid solutions, as it is in the alloys between gold and silver. Unfortunately, such systems are rarely formed in practice, and the scientists are limited by the boundaries of the natural chemical reactions in the materials they investigated. A schematic representation of the tendency for formation of solid solutions in all binary intermetallic systems can be seen in Chapter 2 "Phase diagrams in alloy systems" of the book "Intermetallic chemistry", edited by R. Ferro and A.

Saccone.[37] Further in our review, we also will offer a more detailed summary and analysis of the boundary solid solubility and compound formation between gold or silver and the p-block elements of interest.

On the other hand, the chemical compounds exhibit typical properties, which differ to some extent from the properties of their consisting elements, and in many cases, the properties of the compounds are even more useful than these of their building elements. For example, the Au_2Bi compound, found in the Au-Bi system, is a superconductor despite the lack of superconductivity in any of its constituting elements.[38] The intermetallic chemical compounds are usually stable in time and more durable toward corrosion, and plenty of them can be found in the silver/gold−p-block metal (Ag(Au)-Me) systems.

Formerly, the bimetallic compounds of silver and gold with the p-block elements ($Ag(Au)_xMe_y$) were widely studied as promising lead-free solders due to their thermal and electrical properties,[39] but for some reason they seem to be neglected for plasmonic purposes.

We analyzed the phase equilibria and the ability for compound formation between silver (gold) and the p-block elements, according to their corresponding phase diagrams, enlisted by Hansen and Anderko,[40] and the references provided in the JCPDS-International Centre for Diffraction Data's database of powder diffraction files. On the basis of the analyzed data, and without a claim of full comprehensiveness, a generalized list of the main phases formed in the Ag(Au)-Me (Me−metals and metalloids under investigation) systems, together with their crystalline structures, is presented in Table 2, where the phases with variable composition are given with their corresponding Greek letter names and compositional and temperature ranges, while the compounds with fixed composition are presented by their stoichiometric formulas. By the means of traditional materials science, adopted by Hansen and Anderko in their handbook,[40] the homogeneity regions in the phase diagrams are abbreviated in correspondence to the Bravais lattice concept as follows: α, boundary solid solutions of initial elements with cubic symmetry; β, γ, and μ, compounds with a cubic syngony; and ζ, ϵ, and η, hexagonal structures (η is usually used for boundary solid solutions with a hcp structure). Many of these compounds, found in the Ag(Au)-Me systems, are electronic phases which form at characteristic ratios of valence electrons to atoms, obeying the Hume−Rothery rule and called Hume−Rothery phases.[41]

Several general notes about the chemical affinity for interaction of the elements in the investigated systems can be extracted from the data in Table 2: (i) none of the investigated systems is of the continuous row of solid solutions type; (ii) the most chemically reactive toward gold and silver are the metals and metalloids from the third, fourth, and fifth periods of the Periodic system of elements (Figure 1); (iii) the solubility of the second element is better in solid silver than into solid gold, as boundary Ag-solid solutions appear in more of the systems and are with wider ranges; (iv) more compounds of the Ag-Me systems are of variable compositions with wider homogeneity regions than those of the Au-Me systems; and (v) gold has a better tendency for compound formation with elements with higher molecular weight (6th period of Periodic system).

These observations are in good agreement with those presented in Chapter 2, "Phase diagrams in alloy systems", of the book *Intermatallic chemistry*,[37] and thus, the conclusions described there about the relation between the electro-

Table 2. Alloys and Compounds in the Ag(Au)–Me Systems with Their Homogeneity Ranges and Crystalline Structure of Indexed Phases (Pearson Symbols and Space Groups)[a]

Ag-	phases	Au-	phases
B	no phases; ref 40, p 7	B	no phases; ref 40, p 186
Al	α_{Ag}, 8.75 at % Al (200 °C) up to 20, 34 at % Al (610 °C); β, 24.5 at % Al (603 °C) to 19.9 at % Al (780 °C) and 30 at % Al (727 °C); μ, 22–27 at % Al at RT up to 23.2 at % Al (448 °C); ζ, 25 at % Al (610 °C); α_{Au} up to 23.8 at % Ag (566 °C); ref 40, p 1 indexed synthetic compositions: Ag$_2$Al (hP (Mg); P63/mmc) [JCPDS 14-0647] Ag$_3$Al (cP (β-Mn); P4132) [JCPDS 26-1330; 28-0034]; (cI (W); Im3m) [JCPDS 28-0033]	Al	α_{Au}, 6 at % Al (300 °C) up to 16 at % Al (545 °C); μ (β), very narrow, 20 at % Au (300 °C), 22 at % Au (525 °C); Al$_3$Au$_8$ (formerly Al$_2$Au$_5$), 27.3 at % Al (up to 575 °C); AlAu, 33.3 at % Al (up to 624 °C); Al$_2$Au, 66.7 at % Al (up to 1060 °C), ref 40, p 68 indexed synthetic compositions: AlAu$_4$ (formerly AlAu$_3$) (cP (β-Mn); P4132) [JCPDS 29-0036] Al$_3$Au$_8$ (formerly Al$_2$Au$_5$) (hR (Au$_8$Al$_3$); R3c) [JCPDS 32-0014; 48-1341] AlAu$_2$ (tI (MoSi$_2$); I4/mmm) [JCPDS 26-1005]; (oP (Co$_2$Si); Pnma) [JCPDS 26-1006] AlAu (mP (AlAu); P21/m) [JCPDS 30-0019] Al$_2$Au (cF (CaF$_2$); Fm3m) [JCPDS 17-0877]
Si	no phases, ref 40, p 51	Si	no phases, ref 40, p 232
Zn	α_{Ag}, ~30 at % Zn (100 °C) up to 40.2 at % Zn (258 °C) and 32.1 at % Zn (710 °C); ζ, ~37–51 at % Zn (100 °C) to 45.6 at % Zn (258 °C) and 58.5 at % Zn (274 °C); β, 45.6 at % Zn (258 °C) to 37 at % Zn (710 °C); γ, 58.5–62.7 at % Zn (300 °C) to 61 at % Zn (661 °C); ϵ, 67.4–87.4 at % Zn (200 °C) to 69.4 at % Zn (631 °C) and 89 at % Zn (431 °C); η_{Zn} 1 at % Ag (150 °C) up to 5 at % Ag (431 °C), ref 40, p 62 indexed synthetic compositions: AgZn (cP (CsCl); Pm3m) [JCPDS 29-1155]; (hP (AgZn); p-3) [JCPDS 29-1156] Ag5Zn8 (cI (Cu$_5$Zn$_8$); I43m) [JCPDS 26-0956] AgZn3 (hP (Mg); P63/mmc) [JCPDS 25-1325]	Zn	α_{Ag}, 15 at % (RT) up to 31 at % Zn (642 °C); α_1, 17 (250 °C), 32 at % Zn (150 °C) to 25 at % Zn (420 °C); α_2, 18–32 at % Zn (RT) up to 25 at % Zn (270 °C); β', 48–52.5 at % Zn (RT) to 36.5 (642 °C), 57 at % Zn (626 °C); γ, 64 at % Zn (150–626 °C), ~83 at % Zn (416–475 °C) to 67 at % Zn (644 °C); γ_1, 65–79 at % Au (515 °C; γ_2, 73–78 at % Au (RT) up to 75 at % Au at 225 °C; Au$_{89}$Zn$_{11}$(ϵ), 89 at % Zn (up to 475 °C); η_{Zn} up to 5 at % Au at 423 °C, not defined, ref 40, p 241 indexed synthetic compositions: Au$_3$Zn (tP; P) [JCPDS 07-0055]; (tI; I41/acd) [JCPDS 29-0652] AuZn (cP (CsCl); Pm3m) [JCPDS 30-0608] AuZn3 (cP (H$_3$U); Pm3n) [JCPDS 12-0084]
Ga	α_{Ag}, 11.8 at % Ga (200 °C) up to 18.7 at % Ga (611 °C); ζ (β), ~28–32 at % Cd (~375 °C) up to ~23 at % Cd (611 °C); ζ' (γ), low temp ζ, both not defined); δ, ~59–61 at % Cd (−100 °C) up to 59 at % Cd (326 °C), not confirmed; η_{Ga} 2 at % Ag (−100 °C) up to 3 at % Ag (25 °C), not defined, ref 40, p 21 indexed synthetic compositions: Ag$_{0.72}$Ga$_{0.28}$ (hP (AgZn); P-3) [JCPDS 28-0432] Ag$_3$Ga (hP (Mg); P63/mmc) [JCPDS 28-0431; 47-0991]	Ga	α_{Au}, 8.6 at % Cd (270 °C) up to 13 at % Ga (455 °C); β, 26.5 at % Cd (275 °C) to 26.1 (351 °C) and 28.6 at % Cd (341 °C), not defined; γ, very narrow, ~30–31 at % Ga (RT, ~280 °C), not defined; AuGa, up to 470 °C; AuGa$_2$, up to 492 °C, ref 40, p 204 indexed synthetic compositions: Au$_2$Ga (oC (AsPd$_2$); A21am) [JCPDS 29-0619] Au$_{0.79}$Ga$_{0.21}$ (hP (Au$_7$Ga$_2$), P62m) [JCPDS 18-0530] Au$_7$Ga$_2$ (hP (Au$_7$Ga$_2$); p-62m; high temp. form) [JCPDS 24-0424] AuGa (oP (MnP); Pbnm) [JCPDS 07-0126] AuGa$_2$ (cF (CaF$_2$); Fm3m) [JCPDS 03-0969]
Ge	α_{Ag}, 1 at % Ge (200 °C) up to 9.6 at % Ge (651 °C) ref 40, p 23	Ge	α_{Au}, 0.2 at % (200 °C) up to 3.2 at % Ge (356 °C), ref 40, p 206
As	α_{Ag}, 4.3 at % As (300 °C) up to 8.8 at % As (595 °C); ϵ, 10–13 at % As; forms peritectically at 595 °C, decomposes eutectoidally at 374 °C, ref 40, p 4 indexed synthetic compositions: Ag$_3$As (hP (Mg); P63/mmc) [JCPDS 28-0109]	As	no phases, ref 40, p 154
Cd	α_{Ag}, 40 at % Cd (100 °C) up to 42 at % Cd (440 °C); β, 48–51 at % Cd (440–470 °C) up to 41–55 at % Cd (736–640 °C); β', low temp, β, (49–50 at % Cd (200 °C)) and ~41 at % Cd (240–230 °C) up to 48–56 at % Cd (440–470 °C); γ, 58–62 at % Cd (436–470 °C) up to 58–63 at % Cd (640–590 °C); γ', low temp, γ; ϵ ~ 70–82 at % Cd (100 °C) up to 65–82 at % Cd (590–343 °C); η_{Cd} 3.1 at % Cd (100 °C) up to 7 at % Cd (343 100 °C), ref 40, p 13 indexed synthetic compositions:	Cd	α_{Au}, 18 at % Cd (270 °C), 23 at % Cd (425 °C) up to 32.5 at % Cd (425 °C); α_1, 24–26 at % Cd (300 °C) to 25 at % Cd (425 °C), incl. Au$_3$Cd; α_2, 25–35 at % Cd (425 °C) to 36 at % Cd (612 °C), ~33 at % Cd (625 °C); β, ~ 45–52 at % Cd (200 °C) to 58 at % Cd (370–516 °C) and ~41 at % Cd (612 °C), incl. AuCd; γ, very narrow, ~63–64 at % Cd (~337 °C), ~63.5–64.5 (~357 °C); γ', low temp, γ; 62–64 at % Cd (300 °C); δ, 60 at % Cd (516 °C) and 65 at % Cd (450 °C) and 61 at % Cd (540 °C); δ', low temp, δ, 62–63 at % Cd (~375 °C); ϵ, 72–76.5 at % Cd (309 °C) to 70 at % Cd (500 °C) and 76 at % Cd (496 °C), incl. AuCd$_3$; ϵ', low temp. ϵ, ~73–76 at % Cd (269 °C), not defined; η_{Cd}, ~2 at % Au (RT) up to 3.5 at % Au (309 °C), ref 40, p 190 indexed synthetic compositions:

Table 2. continued

Ag-	phases	Au-	phases
	Ag$_5$Cd$_8$ (cI (Cu$_5$Zn$_8$); I$\bar{4}$3m) [JCPDS 14-0004]		Au$_{3.09}$Cd$_{0.91}$ (tP (α_1); P4/mmm) [JCPDS 05-0676]
	AgCd (oC (AgCd); Cmcm, low temp. phase) [JCPDS 12-0471]; (cP (CsCl) Pm3m) [JCPDS 28-0197]; (hP (Mg); P63/mmc) [JCPDS 28-0198]		Au$_2$Cd (hP (Mg); P63/mmc) [JCPDS 05-0683]
	AgCd$_3$ (hP (Mg); P63/mmc) [JCPDS 28-0199]		Au$_3$Cd$_5$ (tI (Si$_3$W$_5$); I4/mcm) [JCPDS 33-0588; 47-0985]
			AuCd (hP (AuCd); P31m) [JCPDS 05-0675]; (hP (AuCd) P31m) [JCPDS 26-0256]; Au$_{0.51}$Cd$_{0.49}$ (oP (AuCd); Pmmb) [JCPDS 26-0257]; Au$_{0.54}$Cd$_{0.46}$ (oP; Pmcm) [JCPDS 05-0679]; Au$_3$Cd$_{0.97}$ (mP (LiSn); P2/m) [JCPDS 33-0589]
			AuCd$_3$ (hP (Cu$_3$P); P63 cm) [JCPDS 31-0226]; (tI (Pa); I4/mmm) [JCPDS 44-1034]
In	α_{Ag}, 19.1 at % In (0 °C) up to 20 at % In (693 °C); β, 23.7 (667 °C), 24.8 (660 °C) up to 24 at % In (693 °C); ζ, 24 at % In (484 °C) up to 281 °C) up to 23.1 at % In (667 °C), ζ', low temp. ζ (24–26 at % In (from 0 to 187 °C), not defined; γ, 33–34 at % In (0 °C) up to ~310 °C), γ', low temp. γ (0–204 °C), not defined; ψ, 66 at % In (0–166 °C) to 67 at % In (0–141 °C), not defined, ref 40, p 26	In	α_{Au}, 10.4 at % In (400 °C) up to 12.6 at % In (647 °C); ζ, ~16–21 at % In (RT) up to 19 at % In (647 °C); γ, 29.5 (373 °C), 30.5 at % In (647 °C) (364 °C) to 29 at % In (484 °C) and 32 at % In (451 °C); γ', low temp γ (29.5–30.5 at % In (RT) up to 373–364 °C); δ, suggested part of γ, very narrow (~26–27 at % In (482–484 °C) up to 26.5 at % In (488 °C), not confirmed; AuIn, narrow homogeneity region (49.1–50.3 at % In (RT) to 50 at % In (506 °C); AuIn$_2$, 66.7 at % In (up to 544 °C), ref 40, p 210
	indexed synthetic compositions:		indexed synthetic compositions:
	Ag$_9$In$_4$ (cP (Al$_4$Cu$_9$); P$\bar{4}$3m) [JCPDS 29-0678; 71-0128]		Au$_4$In (hP (Mg); P63/mmc) [JCPDS 10-0211]
	Ag$_3$In (hP (Mg); P63/mmc) [JCPDS 29-0677]		Au$_3$In (hP (Ni$_3$Sn); P63/mmc) [JCPDS 42-0800]
	AgIn$_2$ (tI (Al$_2$Cu); I4/mcm) [JCPDS 25-0386]		Au$_7$In$_3$ (hP (Au$_7$In$_3$); P-3) [JCPDS 29-0647; 29-0648]
			Au$_3$In$_2$ (hP (Al$_3$Pt$_2$); P3m1) [JCPDS 26-0710]
			Au$_{11}$In$_3$ (oC (Cu$_{11}$Sb$_3$); Cm2m) [JCPDS 42-0822]
			Au$_{10}$In$_3$ (hP (Au$_{10}$In$_3$); P-3) [JCPDS 42-0821]
			AuIn$_4$ (cP (Cu$_9$Al$_4$); P$\bar{4}$3m) [JCPDS 30-0604; 31-0564; 71-0127]
			AuIn$_2$ (cF (CaF$_2$); Fm3m) [JCPDS 03-0939]
Sn	α_{Ag}, 9.35 at % Sn (218 °C) up to 11.5 at % Sn (724 °C); ζ, 11.8–18 at % Sn (200 °C), 22.85 at % Sn (480 °C), 12 at % Sn (724 °C); ϵ, 23.7–25 at % Sn (200 °C) up to 25 at % Sn (480 °C), ref 40, p 52	Sn	α_{Au}, 5 at % Sn (300 °C) up to 6.8 at % Sn (498 °C); ζ, 12–16 at % Sn (100 °C) up to 13 at % Sn (498 °C); AuSn, 50 at % Sn (up to 418 °C); AuSn$_2$, 66.7 at % Sn (up to 309 °C); AuSn$_4$, 80 at % Sn (up to 252 °C); α_{Sn}, up to ~0.2 at % Au (217 °C), ref 40, p 232
	indexed synthetic compositions:		indexed synthetic compositions:
	Ag$_4$Sn (hP (Mg) P63/mmc) [JCPDS 29-1151]		Au$_5$Sn (hR (Au$_5$Sn); R3) [JCPDS 31-0568]
	Ag$_3$Sn (oP (Cu$_3$Ti); Pmmn) [JCPDS 44-1300; 71-0530]		AuSn (hP (AsNi); P63/mmc) [JCPDS 08-0463]
			AuSn$_2$ (oP (AuSn$_2$); Pbca) [JCPDS 28-0440]
			AuSn$_4$ (oC (PtSn$_4$); Aba2) [JCPDS 28-0441]
Sb	α_{Ag}, 5.5 at % Sb (300 °C) up to 7.2 at % Hg (702 °C); ζ, 8.6–15.6 at % Sb (300 °C) up to 8.8 at % Sb (702 °C), 16.3 at % Sb (558 °C); ϵ, ~22–25 at % Sb (300 °C) up to 18.1 at % Sb (558 °C), 26.6 at % Sb (485 °C); ϵ', low temp. ϵ up to ~440–449 °C, not defined, ref 40, p 48	Sb	α_{Au}, 0.34 at % Sb (300 °C) up to 1.12 at % Sb (600 °C); AuSb$_2$, 66.7 at % Sb (up to 460 °C), ref 40, p 230
	indexed synthetic compositions:		indexed synthetic compositions:
	Ag$_{0.883}$Sb$_{0.117}$ (hP (Mg); P63/mmc) [JCPDS 25-0054]		AuSb$_2$ (cP (FeS$_2$); Pa3) [JCPDS 08-0460]
	Ag$_3$Sb (oP (Ag$_3$Sb); Pm2m) [JCPDS 02-1123]		
Te	Ag$_2$Te (phase transition at 132–145 °C), ref 40, p 55	Te	AuTe$_2$, 66.7 at % Te (up to 464 °C), ref 40, p 234
	indexed synthetic compositions:		indexed synthetic compositions:
	Ag$_2$Te (mP (Ag$_2$Te); P21/n) [JCPDS 34-0142; 42-1266]; (mP (Ag$_2$Te); P21/c) [JCPDS 73-1755; 81-1820]; (cF (CaF$_2$; Cu$_2$Se); Fm3m–high temp. phase) [JCPDS 06-0575; 45-1305; 81-1821; 81-1822]		AuTe$_2$ (mC (AuTe$_2$); C2/m) [JCPDS 79-0191; 81-1067; 81-1068; 81-1069; 81-1070; 81-1071; 81-1072]; (hP (CdI$_2$); P$\bar{3}$m1) [JCPDS 81-1073; 81-1074; 81-1075]; (thin film) [JCPDS 38-0875]
Hg	α_{Ag}, 36.3 at % Hg (100 °C) up to 37.3 at % Hg (276 °C); ϵ (β), ~44–45 at % Hg (0 °C) up to 44.65 at % Hg (276 °C); γ, 55–57 at % Hg (0 °C) up to 56 at % Hg (127 °C); n_{Hg}, 0.06 at % Ag (20 °C) up to 0.93 at % Hg (200 °C), ref 40, p 24	Hg	α_{Au}, ~15–17 at % Hg (100 °C) up to ~19 at % Hg (400 °C); β, 22–27.5 at % Hg (−100 °C) up to 25 at % Hg (−100 °C); Au$_2$Hg, 33.3 at % Hg (420 °C); Au$_2$Hg$_3$, 66.7 at % Hg [liquid phase (up to −36 °C); low temp. phase (122–310 °C); high temp. phase (−36–122 °C)], ref 40, p 207
	indexed synthetic compositions:		indexed synthetic compositions:
	Ag$_3$Hg$_2$ (oC (U); Amam) [JCPDS 27-0617]		Au$_3$Hg (cF (Cu); Fm3m) [JCPDS 04-0781]

Table 2. continued

Ag-	phases	Au-	phases
	$Ag_{1.1}Hg_{0.9}$ (hP (Mg); P63/mmc) [JCPDS 27-0618]; $Ag_2Hg_{3.02}$ (cI (Ag_2Hg_3); I23) [JCPDS 71-0529]		Au_2Hg (hP?) [JCPDS 19-0522]; Au_6Hg_5 (hP (Nb_5N_6); P63/mcm) [JCPDS 26-0715]; $AuHg_2$ (undecided structure) [JCPDS 04-0780]
Tl	$\alpha_{Ag'}$ 2.3 at % Tl (150 °C) up to 7.5 at % Tl (600 °C) [33, p 60]	Tl	$\alpha_{Au'}$ 0.17 at % (200 °C) up to 0.9 at % Tl (800 °C) ref 40, p 239
Pb	$\alpha_{Ag'}$ 0.19 at % (300 °C) up to 2.8 at % Pb (600 °C), ref 40, p 40	Pb	Au_2Pb, 33.3 at % Pb (up to 418 °C); $AuPb_2$, 66.7 at % Pb (up to 254 °C), ref 40, p 223; $AuPb_3$, 75 at % Pb (up to 221 °C), ref 42; indexed synthetic compositions: Au_2Pb (cF (Cu_2Mg); Fd3m) [JCPDS 28-0436]; $AuPb_3$ (tI (V3S); $I\bar{4}2m$) [JCPDS 25-0366; 26-0711]
Bi	$\alpha_{Ag'}$ 0.3 at % Bi (200 °C) up to 2.7 at % Bi (550 °C), ref 40, p 10	Bi	Au_2Bi, 33.3 at % Bi (up to 373 °C), ref 40, p 188, cF (Cu_2Mg); Fd3m [JCPDS PDF 09-0057]

*a*Metastable phases and natural minerals are not included.

negativity, Mendeley number, the Mediema model, and the ability for mutual interactions between the investigated binary systems may be used for further analyses.

To conclude this section, it can be stated that the Ag(Au)-Me systems provide a large number of potential plasmonic compounds, and the homogeneity ranges of some of them (usually the Hume−Rothery electronic compounds) allow an easy way for precise tuning of the desired plasma frequency.

4. PREPARATION OF INTERMETALLIC AG(AU)$_X$ME$_Y$ COMPOUNDS

Basically, all physical methods for synthesis and sintering are applicable for preparation of bulk Ag(Au)-Me compounds. They are easy to obtain due to the common affinity between the metals involved causing a rapid chemical reaction, in some cases even at solid-state.[43] Thanks to the relatively low melting temperatures of the p-block metals, they act as a solvent to the noble metals by forming a rapidly growing interface of the intermediate compound,[44] therefore, the solid−liquid approach for physical synthesis is particularly appropriate. Depending on the tendency toward oxidation of the interacting elements and the intermediate phases formed, in some cases, the smelter has to be insulated from the surrounding air by applying a flux on top of it or by performing the synthesis under vacuum or in an inert gas medium. A profound description of almost all common methods for preparation of intermetallics can be seen in Chapter 6, "Laboratory Preparation of Intermetallic Phases".[37] The more complicated step in the obtaining of a given intermetallic compound is how to keep its desired stoichiometry and crystalline orientation after the synthesis.

As it can be seen from the phase diagrams review (Table 2), the compounds from the Ag(Au)-Me systems are formed by peritectic or peritectoid reactions, often overlapped by composition, exist only in defined temperature ranges, and thus are sometimes unstable at room temperature. This complicates their obtaining by standard uninterrupted reactions and requires conditions for "frosting" of the alloy to its current structural arrangement. Such approach is the thermal annealing at the temperature of the desired equilibrium phase for a long period of time, followed by a sharp quenching of the smelter, usually used for preparation of bulk metastable phases. Most of the electronic phases from the Au-Cd[45] and Au-In,[46−48] as well as the nonexisting in normal conditions metastable phases in the Ag-Te,[49,50] Al-Au,[51] Au-Si,[52] Ag-Ge,[53] and Au-Ge[54−56] systems, were prepared by this approach.

On the other hand, the thermal preparation (physical deposition, chemical synthesis) of bimetallic thin films and nanoparticles offers exactly what is needed by giving the desired energy to the elements by treatment at a given temperature and realization of an abrupt termination of the process. In the cases of direct (physical) preparation, which include practically all physical vapor and plasma deposition methods, the energy for reaction is acquired by precise tuning of the heating temperature (evaporation rate) or the ablation power for vapor and plasma methods, respectively, while the quenching is naturally realized by condensation of small quantities of the materials on a much colder surface. When an indirect (chemical) approach is used, which includes the different types of chemical vapor deposition (CVD) methods and the approaches of the soft chemistry, the energy for reaction and the "frosting" of the product are given either

through temperature variations or by the inset of a certain chemical additive. Furthermore, in order to meet the strict requirements, in terms of particles' dimensions and perfection, needed for successful optical and plasmonic applications, the methods for thin film deposition and nanoparticles' synthesis seem to be the most appropriate.

This wide variety of approaches for preparation of binary Ag(Au)-Me alloys and compounds is applied in the preparation of samples for optical and electrical studies, without any being of particular preference. In general, for evaluation of the overall SPR excitation without disturbance from its localization, the samples should be thick enough and with natural grain sizes. Therefore, bulks or relatively thick-layer specimens are used for these purposes. Some bulks are polycrystalline, prepared by direct synthesis of elements,[57−61] others are monocrystalline, obtained by the means of Bridgman and zone melting technologies.[62−64] But most of the samples are in the form of polycrystalline layers, prepared by almost all possible physical methods for deposition, as thermal deposition in vacuum,[35,65−68] arc melting,[69] laser ablation,[70] magnetron sputtering,[71−73] ion implantation,[74] etc., either from preliminary synthesized bulks or from the initial elements, as the last are either coevaporated[35,65−68] or deposited by alternating layered structures.[66,68,75,76] The chemical reactions for formation of the desired compounds are realized either by solid-state self-assembly of the components[66,77] or by further thermal annealing.[59,68,78]

Although our review is not pointed directly toward Ag(Au)-Me intermetallic compounds of a particular size and shape, due to the lack of enough compatible data in the literature, we will make a short summary of the possible methods for preparation of more complicated binary intermetallic structures (core−shell nanoparticles, hollow core nanoshells, nanoparticles with a precise shape, etc.), as they are of particular importance for the excitation of a quality LSPR signal needed for actual applications.[79] Generally, the possibilities offered by the soft chemical methods are more preferred for these purposes. M. Zhou et al.[80] show a good review on the general principles for formation of nanoalloys, the methods for their preparation, and the possibilities for their application. Cortie and McDonagh[81] describe some methods for preparation of hybrid plasmonic nanostructures in particular, as deposition of the first component followed by precipitation of the second on top; galvanic replacement through precipitation of a second component and coprecipitation of the two materials, which may be also applied for preparation of intermetallic compounds. Loza et al.[82] point that the coprecipitation (from the chemical methods) and the laser ablation (from the physical ones) cause alloying of the elements in the nanoparticles, while the seeded growth mechanism and the galvanic replacement lead to formation of core−shell nanostructures and hollow core nanoshells, respectively. The polyol method for synthesis of noble metal nanoparticles is getting extremely popular these days due to its relatively easy and accessible realization and the possibility for preparation of equal nanoparticles with precise shapes.[83] A good review on the preparation of nanodimensional intermetallic compounds, represented by specimens from the Ag−Zn system, using a one-pot synthesis from solutions, and the influence of the different dissolving agents on the shape and the dimensions of the resultant nanoparticles, is given by Schaefer et al.[84] The preparation of different crystalline and compositionally uniform intermetallic nanocrystals of Au-Ga, Ag-Ga, Cu-Ga, Ni-

Ga, Pd-Ga, Pd-In, and Pd−Zn compounds by the colloidal synthesis method is demonstrated in the review of Clarysse et al.[85] The fundamental advantage of this method is that it achieves compositional tunability across the phase spaces (e.g., $AuGa_2$, AuGa, Au_7Ga_2, and Ga-doped Au), size tunability (e.g., 14.0, 7.6, and 3.8 nm $AuGa_2$), and size uniformity (e.g., 5.4% size deviations). Synthesis of nanoparticles by laser ablation or Ag, Au, and In colloids are described in papers.[86,87]

A summary of the references describing the methods used for the preparation of particular Ag(Au)-Me alloys and compounds for optical applications, which were presented in this section, is given in Table 3. However, taking into account

Table 3. Summary of the Preparation Methods of Ag(Au)-Me Alloys, Referred to in Section 4, Divided According to the General Form of the Resultant Specimens (Bulks, Thin Films, and Separate Nanoparticles)[a]

system	materials and methods	system	materials and methods
Ag-Al	bulks: DS[58]	Au-Al	bulks: ZM[64]
	thin films: MS;[71,72] AlterLD[76]		thin films: AM[69]
Ag-Zn	bulks: DSTA[78]	Au-Zn	—
	nanoparticles: OPS[84]		—
Ag-Ga	thin films: SSSA[77]	Au-Ga	nanoparticles: CS[85]
	nanoparticles: CS[85]		—
Ag-Cd	bulks: DS;[61] DSTA[78]	Au-Cd	—
Ag-In	bulks: DS[57,58]	Au-In	thin films: CE;[66,67] SSSA/AlterLD[66]
	thin films: CE;[35,65] AlterLD[75]		nanoparticles: LA[87]
	nanoparticles: LA[86,87]		—
Ag-Sn	bulks: DS[58,60,61]	Au-Sn	nanoparticles: PP[83]
	thin films: TDV[66]		—
	nanoparticles: PP[83]		—
Ag-Sb	thin films: CE;[65] MS;[73] II[74]	Au-Sb	bulks: BM[62]
Ag-Te	bulks: BM[63]	Au-Te	—
Ag-Bi	thin films: CE;[68] AlterLDTA[68]	Au-Bi	—

[a]DS, direct synthesis; DSTA, direct synthesis with further thermal annealing; ZM, zone melting; BM, Bridgman method; TDV, thermal deposition in vacuum; MS , magnetron sputtering; CE , coevaporation; AlterLD , alternating layers' deposition; AlterLDTA , alternating layers' deposition with further thermal annealing; AM, arc melting; II, ion implantation; LA, laser ablation; SSSA, solid-state self-assembly; OPS, one-pot synthesis; CS, colloidal synthesis; and PP, polyol process.

the already mentioned affinity of the noble metals to react with the p-block elements and the fundamental literature on the synthesis of alloys, it should be noted as a conclusion that all methods, both physical and chemical, are appropriate for the preparation of Ag(Au)-Me alloys when proper attention on the conditions for interruption of the growth process is taken into account.

5. OPTICAL PROPERTIES OF SOLID SOLUTIONS OF SILVER AND GOLD WITH P-BLOCK METALS

The possibility to control the plasmonic properties of solid solutions, as in the case of the Ag−Au system, is the reason for the research interest to these parts of the Ag(Au)-Me phase diagrams. The most frequently used criteria for evaluating the efficiency for SPR and LSPR excitation are the coefficients Q_{SPR} and Q_{LSPR}, which are defined as the following ratios of the

real and imaginary part of the complex permittivity $\varepsilon = \varepsilon' + i.\varepsilon''$:[31,88]

$$Q_{SPR} = \varepsilon'^2/\varepsilon'' \text{ and } Q_{LSPR} = -\varepsilon'/\varepsilon'' \qquad (1)$$

The influence of interband transitions on the excitation efficiency of localized plasmon resonance was evaluated, with Q_{SPR} and Q_{LSPR} being represented by the parameters of the Drude dispersion formula:[31]

$$Q_{LSPR}^{max} = \frac{2(\omega_p^2 - \Gamma^2)^{3/2}}{3\Gamma\omega_p^2\sqrt{3}}, \qquad Q_{SPR}^{max} = \frac{\omega_p^2}{2\Gamma^2} \qquad (2)$$

These parameters are related to the temperature-dependent DC resistivity, ρ_{DC}, and the permittivity of free space, ε_0, by the following equation:[31]

$$\Gamma = \varepsilon_0 \cdot \omega_p^2 \cdot \rho_{DC} \qquad (3)$$

Blaber et al.[31] introduced a second criterion for a high-quality plasmonic material: the number of electrons involved in interband transitions must be low and at the highest possible frequency. This criterion significantly reduces the number of materials that are likely to have favorable plasmonic properties. Due to the interband transitions in the visible spectral range and low frequency effect on the polarizability, all materials with partially occupied d or f electronic states are going to perform poorly as plasmonic materials. Moreover, although the quality factor Q_{LSPR} is widely used, it does not give a full and quantitative picture of the plasmonic performance of a material. Thus, the Faraday (Fa) and Joule (Jo) factors have been introduced by Lalisse et al.[88] to represent the optical near field enhancement and photothermal conversion efficiency, respectively. According to Toudert et al.,[89] Fa and Jo are more suitable to evaluate quality of LSPR in the case of the interband plasmonic resonances.

The complex permittivity of the alloys of silver and p-block metals with compositions that fall into the range of solid solutions has been studied for the following systems, Ag-Al (up to 12 at. % Al),[71,72,90] Ag-Zn (up to 30 at. % Zn),[78] Ag-Cd (up to 12 at. % Cd),[78] Ag-In (up to 12 at. %),[35,57,65] and Ag-Sb (up to 2 at % Sb).[65] In the reflection spectra in the case of α-phase (silver-based solid solution), a shift of the minimum due to the longitudinal oscillations of the electron plasma, or the so-called volume plasmon resonance, is observed. In the case of the Ag—Al system a shift toward the shorter wavelengths from 320 to 300 nm at aluminum content of 5 at % is registered.[71] This effect is accompanied by a shift of the region of high reflectance to the longer wavelengths in the infrared spectral region.

The published spectra of the real part of the complex dielectric function show that upon addition of small amounts of up to 5 at. % Zn, Cd, and Al, a shift of the ε' spectra to lower photon energies is obtained.[78,90] Along with this shift, there is a shift of the point where the values of ε' change their sign from negative to positive, i.e., $\varepsilon' = 0$. At content of Al and In higher than 5 at %, the position of the $\varepsilon' = 0$ cross-point begins to shift toward the higher photon energies. The published results of the aforementioned systems[78] show that when the p-metal content is equal to or greater than 10 at %, the ε' keeps its negative value in a wide spectral range from 0.5 to 6.5 eV, which indicates a shift of the screen plasmon frequency at the deep UV range.

In the imaginary part of complex permittivity, ε'', there is an increase of its values for photon energies lower than 3.9 eV and a decrease of ε'' for photon energies greater than 4.0 eV. This effect is demonstrated in Figure 2a, where a comparison of
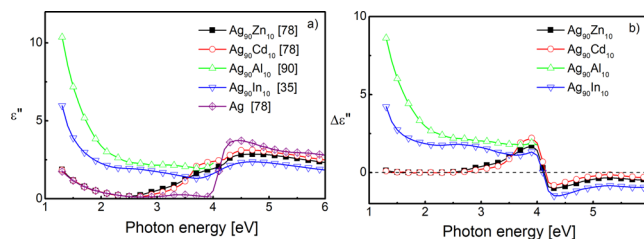

Figure 2. Comparison of literature data for ε'' for silver-based solid solutions with Zn,[78] Cd,[78] Al,[90] and In[35] (a), and variation of $\Delta\varepsilon''$, differences of ε'' of these solid solutions with respect to ε'' of silver[78] (b). Numerical data from the mentioned references was used for the plots of ε'' and calculation of $\Delta\varepsilon'$.

literature data[35,78,90] is shown for solid solutions based on silver with Cd, Zn, Al, and In. Figure 2b shows their differences with respect to ε'' of silver, $\Delta\varepsilon''$. It can be seen that in the UV spectral region, for photon energies greater than the plasmon frequency of silver, the values of ε'' decrease, with the most significant changes in the case of $Ag_{90}In_{10}$ thin film. These changes in the ε'' spectra are due to an increase of the energy for transitions from the 4d band of silver to the Fermi level L3-L2' and a decrease of the energy for transitions from the Fermi surface to the s-band (L2'-L1) of silver.

At a higher content of dopant elements, the appearance of a low-energy peak is observed. The comparison of the published spectra of ε'' shows that the maximum of this band shifts from 3.79 to 3.10 eV as the zinc content increases from 10 to 30 at %, while in the Ag—Cd alloys, this shift is more significant, from 3.85 to 2.85 eV at the same variation of the cadmium content. Furthermore, the intensity of this peak is also higher in the case of Ag-Cd than the Ag-Zn alloys. According to the authors,[78] the reason for this effect is that the $4s^2$ electrons of Zn are more strongly bound and they remain localized, while the cadmium $5s^2$ electrons are more active. The addition of an electron by the Cd atom contributes to the total number of electrons, thereby raising the Fermi level by placing electrons in normally vacant energy states, where they may contribute to the transition from the Fermi level to the s band.[78] In the ε'' spectra of thin Ag—Al and Ag—In films with Al and In content greater than 5 at %, a peak appears in the spectral region of 2.5—2.7 eV.[35,78] Green et al.[78] suggest that this peak is due to transitions of the p electrons of aluminum to the free and occupied s states of silver.

The analysis of the properties of the silver-based solid solutions show that the addition of p-block metal in silver results in a shift of the screen plasmon frequency to the higher photon energies in the ultraviolet spectral region. Since the volume plasmon is associated with longitudinal oscillations of the electrons, its frequency can be clearly observed in the spectra of the so-called dielectric loss function. From the published loss function results of Ag—Al,[90] Ag—In,[35] and Ag—Sb,[65] a shift to higher photon energies is seen, but at the same time, the intensity decreases and the peak width increases. Although the values of ε'' decrease for the considered α-phases in the UV spectral region, and the values of ε' are negative, their small absolute values result in not very high values of the Q_{LSPR} parameter in the UV.

Table 4. Summary of Literature Data on Optical Properties (Reflectivity, R, Refractive Index, n, Extinction Coefficient, k, and Complex Permittivity, ε) and Plasmonic Properties (Crossover Point of Real Part of Complex Permittivity ($\varepsilon' = 0$), ω_s, Coefficient of Efficiency for LSPR Excitation Q_{LSPR} and Cross-Section of Extinction, σ_{ext}) of Ag-p-Block Intermetallic Solid Solutions for Bulk Samples (B) and Thin Films (TF)[a]

system	sample	method of preparation	available optical data and spectral range	composition of the investigated samples	ω_p (eV)	ω_s (eV)	$\sigma_{ext}/\omega(\sigma_{ext})$ (eV)	ref.
Ag-Zn	B	DS	R, ε (1–7 eV)	$Ag_{96}Zn_4$	n.a.	~3.65 eV	n.a.	78
				$Ag_{70}Zn_{30}$	n.a.	$\varepsilon' < 0$ ($h\nu$ = 1–7 eV)	n.a.	
Ag-Cd	B	DS	R, ε (1–7 eV)	$Ag_{96}Cd_4$	n.a.	~3.75 eV	n.a.	78
				$Ag_{90}Cd_{10}$	n.a.	~4.05 eV	n.a.	
				$Ag_{70}Cd_{30}$	n.a.	~6.2 eV	n.a.	
Ag-Al	TF	CD-DCMS	ε (0.72–6.2 eV)	Ag_xAl_{1-x} ($x > 0.35$)	n.a.	red shift of ω_s from ~3.2 eV to ~1.80 eV	n.a.	93
	TF	CD-DCMS	R, ε (0.4–4 eV)	Ag_xAl_{1-x} ($x > 0.875$)	n.a.	Al increases the Ag frequencies of longitude electron oscillations from 3.8 eV to ~4.0 eV	n.a.	90
Ag-In	B	Ames Laboratory	ε (0.6–6.5 eV)	$Ag_{98}In_2$	7.9	n.a.	n.a.	57
				$Ag_{88}In_{12}$	6.91		n.a.	
	TF	CD	ε (0.6–6.5 eV)	Ag_xIn_{1-x} ($0.9 \leq x \leq 1$)	–	blue shift of ω_s from ~3.8 eV to ~4.1 eV	–	35
				$Ag_{98}In_2$	9.19		4800/3.2	
				$Ag_{90}In_{10}$	6.63		~6700/3.15	
Ag-Sb	TF	CD-TCE	ε (0.6–6.5 eV)	$Ag_{98}:Sb_2$	4.10	n.a.	n.a.	65
Ag-Bi	TF	CD-TCE AlterLD	R, ε (0.6–6.5 eV)	Ag_xBi_{1-x} ($x = 0-1$)	3.83–10.85	~1.5–6.2 eV	n.a.	68

[a]DS, direct synthesis; CD, codeposition (CD-DCMS codeposition by DC magnetron sputtering; CD-TCE codeposition by thermal coevaporation); AlterLD, alternating layers' deposition; and $h\nu$, spectral range.

The interband transitions in these silver alloys are similar to the analogous copper alloys. A comprehensive study of the band structure of copper alloys doped with Zn, Ga, and Al[91] shows that the interconduction band threshold tends to a common value of about 2.5 eV. At higher concentrations of the p-block metal in silver-based alloys Ag-Me (Me = Al, In, Sn, Sb), the regions of the intermetallic compounds appear and mostly hexagonal structures are observed (Table 2). Despite the greater resistivity, these phases can have greater hardness, which find application as electrical contact materials with enhanced tribological properties.[58,73]

The optical properties of gold-based solid solutions with p-block metals have not been investigated. Shiraishi et al.[59] showed that in Au−Pt alloys with a gold content of 86−88 at %, the addition of indium to ~4 at % minimizes the reflection coefficient associated with the plasmon frequency at lower photon energies. Due to the change of the plasmon frequency, the intermetallic alloys and compounds change their color, which is the reason why they find applications not only in the areas described above but also in jewelry[92] and in stomatology as material for preparation of dental prostheses.[59]

As was shown in Table 2, some metals, such as Bi and Ge, form only heterogeneous alloys with silver and gold, and thus their resistivity can be expected to increase with an increasing doping element. The published values for electrical resistivity ρ of Ag-Ge alloys are in the range from 17 to 70 $\mu\Omega$ cm and have a maximum at 30 at % Ge,[62] which is near to the eutectic point (26 at % Ge) in this system,[40] which in general causes formation of more disordered and defect structures. For those intermetallic systems, in which heterogeneous mixtures are formed, a better efficiency can be expected at smaller concentrations of the additional element.

An overview of the existing data on the optical and plasmonic properties of the Ag-p-block metal solid solutions is presented in Table 4.

In conclusion, the analysis of the existing studies of solid solutions based on silver and p-block metals (Cd, Zn, Al, and In) demonstrates that the doping of silver with p-block metals shifts its plasma frequency toward higher photon energies in the UV spectral region. Unfortunately, the difference in the crystal lattices of the noble metals and the p-block metals leads to two effects: due to the limits of the solid solutions regions in the phase diagrams, the maximal concentration of the diluted p-element for each period of the Periodic table of chemical elements decreases with increasing number of valence electrons (see Table 2). The second effect is that the increase of the p-block metal concentration leads to an increase of the crystalline disorder and therefore decreases the efficiency for excitation of surface plasmon resonance.[31] We will address this problem at the beginning of the next part. The compositional limitations of the boundary solid solutions cause limitations in their applicability as effective plasmonic materials in the UV spectral region for photon energies less than 3.5−6 eV (see Table 4).

6. OPTICAL PROPERTIES OF INTERMETALLIC COMPOUNDS

As has been pointed out in section 5 of the present review, the excitation efficiency of SPR and LSPR depends on the ratio parameters of the Drude dispersion formula, ω_p/Γ, which is related to the temperature-dependent resistivity of the material.[31] Therefore, in the absence of plasmonic activity data, conductivity data can be used to estimate Q_{SPR} and Q_{LSPR}. Equation 3 shows that a decrease in the values of ρ_{DC} leads to an increase in the ratio of ω_p^2/Γ, and from these values an estimate can be made of the efficiency of excitation of surface plasmon resonance.

Figure 3 shows the compositional dependence of ρ_{DC} for the Ag-In and Ag-Sn systems, using published numerical data.[92,94] In the case of Ag-In solid solutions, the resistivity was
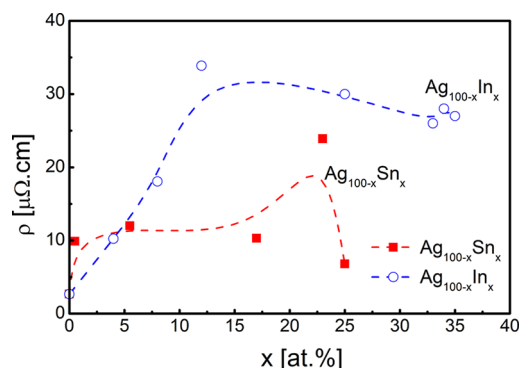
Figure 3. Variation of resistivity of Ag−In and Ag−Sn thin films in concentration diapason 0−35 at %. Reference numerical data for the Ag-In[57,60] and Ag-Sn[61,96,97] systems was used for the plots.

calculated using eq 3 and the values for ω_p and Γ, given by Kim et al.[57]

The studies of the conductivity of Ag-In alloys situated between the intermetallic compounds Ag_3In and Ag_9In_4[60,95] show a decrease in resistivity for the compositions close to the Ag_9In_4 intermetallic phase. It is also seen in Figure 3 that the resistivity in the case of Ag-In alloys increases when the indium content increases from 0 to 25 at %. The solid solution conductivity of the Ag-Sn system shows that ρ increases from 9.9 $\mu\Omega$ cm to 12 $\mu\Omega$ cm when the Sn content increases from 0.5 to 5.5 at %.[61,96] Even higher values are observed in the case of thin films with tin content between 10 and 20 at %,[97] where the homogeneity region of the hexagonal ζ phase is situated. A sharp decrease in resistivity is observed in the ordered intermetallic phase, Ag_3Sn, 6.8 $\mu\Omega$ cm. To summarize these observations, it can be said that the formation of ordered intermetallic crystalline phases, such as Ag_3In, Ag_9In_4, and Ag_3Sn, leads to a decrease in their resistivity, and since $1/\rho_D \sim \omega_p^2/\Gamma$, one can expect an increase in efficiency for the excitation of SPR and LSPR in them.

The published data reports resistivity values of the intermetallic compounds: Ag_5Cd_8 (13.1 $\mu\Omega$ cm),[60] Ag_2Al (29.7 $\mu\Omega$ cm),[60] $AuSb_2$ (25 $\mu\Omega$ cm),[98] which are significantly lower than those of the intermetallic compounds of silver and gold with alkali metals (which range between 7.6 and 117 $\mu\Omega$ cm and possess relatively high values of $Q_{LSPR} \sim 50$),[20] and therefore, an even higher efficiency for the excitation of LSPR can be expected for these compounds.

As it was shown up to here, the higher order of the intermetallic crystalline compounds can improve plasmon efficiency, and it could even be greater than this of heavily doped silver-based solid solutions of the p-block elements. The optical properties of the intermetallic phases are studied in presynthesized bulk samples of compounds from the Ag-Zn and Ag-Cd systems,[99,100] in presynthesized crystal samples of $AuAl_2$, $AuGa_2$, $AuIn_2$[101−103] and $AuSb_2$,[104] in the case of the presence of crystalline compounds in thin films from the systems Ag-Ga,[77] Ag-In,[35,65,75] and Ag-Al,[71] as well as in Ag/Sn and Au/In multilayer structures.[66,67]

The elements Zn and Cd from group 12 of the Periodic table are the most active toward compound formation with silver and gold, and all of these compounds are electronic Hume−Rothery phases with variable compositions in wide homogeneity ranges. The optical properties in the Ag-Zn and Ag-Cd systems were studied for the AgZn, Ag_5Zn_8, $AgZn_3$, AgCd, Ag_5Cd_8, and $AgCd_3$ compounds.[100,101] The reflection

spectra of the β-phases of CuZn, AgZn, AgCd, and AuZn show the presence of a minimum in the spectral region 2.4−2.5 eV associated with interband transitions.[99] The color of the β-brass-type alloys CuZn, AgZn, AgCd changes in the order yellow gold-salmon pink-violet. According to the band structure of AgZn and AgCd, presented by Amar et al.,[99] there is an overlapping of the $4d^{10}$ Ag electronic band with the $4s^2$ and $5s^2$ bands of zinc and cadmium, respectively. Consequently, there is a reduction in the energy gap between the 4d level of silver and the Fermi level, and therefore, the minimum in the imaginary part of the complex permittivity, ε'', should be shifted to photon energies lower than those of pure silver. The increase of the number of electrons that participate in the interband transitions with energies falling in the visible spectral region reduces the intensity of the interband transitions in the ultraviolet spectral region. The optical absorption spectra of the Ag_5Cd_8 phase was studied only in the case of nanoparticles[74,105,106] and showed a maximum at a wavelength of 310 nm.

Data on the optical properties of intermetallic crystalline compounds of silver with the group 13 elements can be found about thin films with compositions corresponding to the bulk compounds. From the crystalline phases in the Ag-Ga system, the Ag_2Ga has been investigated in the case of thin films.[77] The complex permittivity spectra, calculated from ellipsometric measurements, show that ε' possesses negative values in a wide region starting from infrared to UV spectral regions. In the spectrum of ε'', a maximum due to interband transitions is observed in the visible spectral region at a photon energy of ~2.0 eV.

A comprehensive study of the compositional dependence of the complex permittivity of thin films with compositions close to the intermetallic compounds Ag_3In, Ag_9In_4, and $AgIn_2$ is seen in the work of Todorov et al.[35] The real part of the complex permittivity of the thin layers is negative in the entire studied spectral interval of 0.6−6.5 eV, which is in agreement with the calculated density of electron states.[107] The dispersion parameters suggest that the values of ε' become positive at higher energies.[35] The analysis of the Lorentzian component of the dielectric function shows intense interband transitions in the visible spectral region in the interval 1.7−2.2 eV. The largest contribution of the interband transitions to the total dielectric function is in the case of a thin film with a composition close to the $AgIn_2$ intermetallic phase, as a result of which the negativity of the real part decreases.[35]

Information on the optical properties of intermetallic compounds of silver with aluminum can be found only in research on the properties of thin films with a high aluminum content of 80 and 90 at %, which represent mixtures containing the phases, Ag_2Al and Ag_3Al, as their influence on the optical properties of the Ag-Al alloys was traced out.[71] The authors observed a maximum in the imaginary part of the complex dielectric function associated with the plasmon frequency of aluminum at a wavelength of 800 nm (1.5 eV), which shifts toward the shorter wavelengths with increasing the silver content. The heating of the thin films leads to a shift of the Lorentz oscillation in the simulation model from 1.647 to 1.512 eV, which according to the authors is due to the appearance of the Ag_2Al phase.[71]

The information about the optical properties of the compounds of silver with the elements of the following groups 14, 15, and 16 from the Periodic system of elements is even

scantier and only partial investigations on the Sn-, Sb-, and Te-containing phases can be found.

The influence of the intermetallic crystalline phase Ag_3Sn is visible in the spectra of complex permittivity of bilayered Sn/Ag and Ag/Sn coatings.[66] The real part of complex permittivity possesses typical negative values in the spectral interval of 0.5−6.5 eV, while the imaginary part decreases with increasing photon energy. The presence of the Ag_3Sn compound in the bilayer coatings shows a broad absorption band located approximately between 1 and 3.5 eV. According to Wronkowska et al.,[66] this band can be attributed to the interband transitions from the Sn bands to the Fermi level or from the valence states to the conduction states in the Ag_3Sn compound.

From the results presented above can be seen that the compounds of silver with the p-block metals are characterized by negative values of the real part of the complex permittivity, ε'. The ε'' possesses higher values in the visible spectral region and decreases in the UV spectral region. In contrast to the intermetallic compounds of Ag with Cd, in whose spectra of ε'' a minimum is observed in the spectral interval 2.3−2.5 eV, in the intermetallic compounds of silver with elements from groups 13−15, the peaks are observed in the spectral region 1−3 eV. The shift of the most intensive interband transitions in the visible range is a reason for lower values of ε'' in the UV region between 3.5 and 6 eV. The different position of the peak is due to the difference in the electronic transitions, which can be seen from the band structure of these compounds, as the considered elements have a different number of p electrons in their last electron shell. The band structure and density of electron states of Ag_3In and $AgIn_2$ are given by Yu et al.[107] An overlap of the 5s and p electron levels of indium with the 4d level of silver creates a broad band of electronic states below the Fermi level and the possibility of orbital hybridization. According to the obtained result, the density of states (DOS) is different from zero at the Fermi level, which determines the metallic character of these crystals.

The tin and antimony contain a larger number of electrons, which leads to an increase in the energy gap between 5s electronic states of these elements and the Fermi level. The calculated band structures of Ag_3Sn[108] and Ag_3Sb[109] show that the 5p electrons of tin and antimony, which lie below the Fermi level, overlap with the 4d band of silver, while the Sn's 5s electronic band is separated by an energy gap of ∼1.5 eV and plays a minor role in the Ag-Sn orbital hybridization.

The Ag_2Te is a narrow band gap semiconductor with two allotropic forms, disordered high temperature α-Ag_2Te and low temperature monoclinic β-Ag_2Te.[110] The investigation of the optical properties of monoclinic Ag_2Te crystals in a wide range (3.7 meV − 6.2 eV) of photon energies is presented by Yeh et al.[63] The β-Ag_2Te phase is characterized by an indirect bandgap (∼10 meV) and a direct bandgap (∼1.84 eV) and plasmon frequency at the far-infrared spectral range ∼50 meV.

The optical properties of the intermetallic compounds of zinc and cadmium with gold, β-AuZn and β-AuCd, were studied in the form of crystal samples by Schaefer et al.[84] In the reflectance spectra of β-AuZn and β-AuCd, a minimum is observed at wavelengths of ∼500 nm and ∼600 nm, respectively. At shorter wavelengths, the reflection coefficient decreases, less significantly than in the case of their silver counterparts. Of the optical properties of intermetallic crystalline compounds of gold with the p-block metals, it mainly turns to those of group 13 of the Periodic system. In

the spectra of complex permittivity of crystals of $AuAl_2$, $AuGa_2$, and $AuIn_2$,[101−103] as well as of thin films and two-layer coatings containing Au_7In_3, AuIn, $AuIn_2$, and Au_3In_2 compounds, a maximum of ε' at photon energies of 1.8 eV is observed, while the imaginary ε'' part is characterized by a maximum within 2.0−2.3 eV due to interband transitions.[66,75]

The $AuAl_2$, $AuIn_2$, and $AuGa_2$ crystals are characterized by unusual purple and blue colors. The understanding of the origin of this color variation is the reason for studying the spectra of complex permittivity and their band structure of $AuAl_2$, $AuIn_2$, and $AuGa_2$ for a long time. $AuGa_2$ and $AuIn_2$ are characterized by negative values of the real part of complex permittivity, ε', in the spectral interval 0.5−6 eV, and they increase with increasing photon energy, while the contribution of interband transitions are the cause of the $AuAl_2$'s ε' to change the sign to positive at photon energy ∼2.3 eV.[101,102] The main plasmon resonance frequencies were found at 7.0, 7.8, and 7.5 eV for the $AuAl_2$, $AuGa_2$, and $AuIn_2$ crystalline phases, respectively.

In the spectra of ε'', a peak related to interband transitions at a higher energy of ∼2.5 eV is observed for $AuAl_2$, and its position shifts toward lower photon energy of ∼1.8 eV in the other compounds ($AuGa_2$ and $AuIn_2$). In the UV spectral region, the values of ε'' for the $AuAl_2$, $AuGa_2$, and $AuIn_2$ crystalline phases decrease. The smallest values are obtained in case of $AuIn_2$, where ε'' decreases from 4.00 to 2.88 in the spectral region of 4−6 eV.[101] The comparison of the optical properties shows that the plasma activity of $AuAl_2$ and $AuGa_2$ crystals is shifted toward longer wavelengths compared to their counterparts containing platinum, $PtAl_2$ and $PtGa_2$.[64] The band structure of $AuAl_2$ shows that the Au 5d band has more atomistic character and does not actively participate in the coloring and optical property of $AuAl_2$.[64]

The spectrum of ε'' of the crystalline $AuSb_2$ phase is characterized with a number of peaks, which are positioned at 0.5, 0.75, 2.2, 3.25, and 4.6 eV and are associated with interband transitions.[104] The band structure of $AuSb_2$ shows that the peaks in the spectrum of ε'' are due to interband transitions with Au s-p and p-d character mixed with Sb's p character lying in the conduction band region. The density of electron states shows that the Fermi surfaces are mainly due to Sb-5p and Au-5d electrons. The Sb-5s states are separated by a gap of 3.8 eV from the Sb-5p and Au-5d electrons and therefore contribute to interband transitions at higher photon energies.[62,111]

Besides the optical properties of crystalline samples and thin films, the multilayer structures, that can be considered as superlattices of silver and p-block metals, can be of practical interest. Published results for Ag/Al,[76] Ag/Bi,[68] and Al−In[112] coatings show that they exhibit an energy shift where the real part of the complex permittivity changes its sign and have potential applications as epsilon-near-zero materials.

The cross-section of extinction, σ_{ext}, is a sum of absorption and scattering. For small particles, the excitation is dominated by the absorption cross-section − $\sigma_{abs} = \frac{k}{\varepsilon_0} Im(\alpha_p)$, while the larger particles' main contribution has a scattering cross-section − $\sigma_{scatt} = (\frac{k^4}{6\pi\varepsilon_0^2})|\alpha_p|$, where $k = 2\pi/a$ is wave vector, ε_0 is the vacuum permittivity, and with $|\alpha_p|$ is denoted the polarizability of a sphere:[113]

$$\alpha_p = 4\pi\varepsilon_0 a^3 \frac{\varepsilon(\hbar\omega) - \varepsilon_m}{\varepsilon(\hbar\omega) + 2\varepsilon_m'} \tag{4}$$
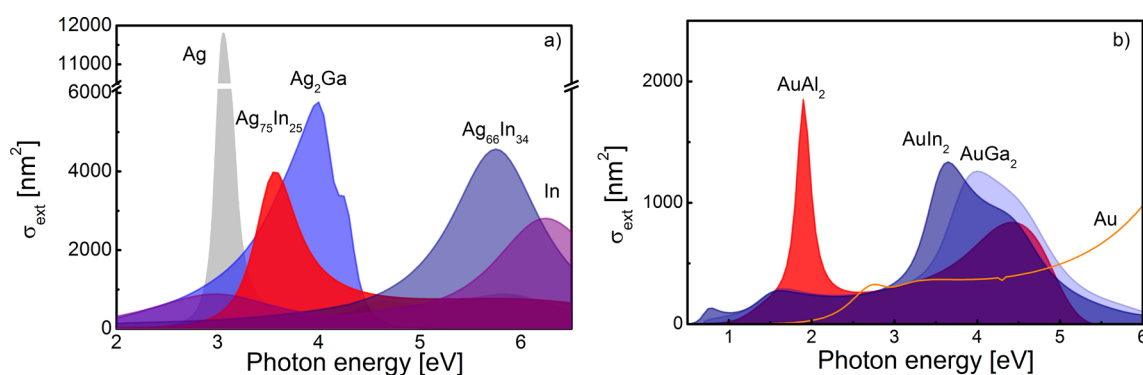
Figure 4. Comparison of the cross-section of extinction σ_{ext} of some intermetallic compounds of silver (a) and gold (b) and p-block metals. Published data[35,77,101,102] were used for calculation of σ_{ext}.

Table 5. Summary of Literature Data on Optical Properties (Reflectivity, R, Refractive index, n, Extinction Coefficient, k, and Complex Permittivity, ε) and Plasmonic Properties (Crossover Point of Real Part of Complex Permittivity ($\varepsilon' = 0$), ω_s, Coefficient of Efficiency for LSPR Excitation Q_{LSPR} and Cross-Section of Extinction, σ_{ext}) of Ag(Au)-p-Block Alloys with Compositions Falling in Regions of Intermetallic Compounds for Bulk Samples (B) and Thin Films (TF)[a]

system	sample	method of preparation	available optical data and spectral range	composition of the investigated samples	ω_p (eV)	ω_s (eV)	$\sigma_{ext}/\omega(\sigma_{ext})$ (eV)	ref
Ag-Zn	B	DS	R (1.8–4.1 eV)	AgZn	n.a.	n.a.	n.a.	99
Ag-Cd	B	DS	R (1.8–4.1 eV)	AgCd	n.a.	n.a.	n.a.	99
Ag-Al	TF	CD-DCMS	ε (0.72–6.2 eV)	Ag_xAl_{1-x} (x < 0.35)	n.a.	ε' < 0 (hν = 0.72–6.2 eV)	n.a.	77
Ag-Ga	TF	Ga ID in Ag TF	ε, n, k (1.4–4.1 eV)	Ag_2Ga	n.a.	>4.13 eV	n.a.	77
Ag-In	TF	CD	ε (0.6–6.5 eV)	Ag_xIn_{1-x} (x = 0–1)	—	ε' < 0 (hν = 0.5–6.5 eV) for $0.25 \leq x \leq 0.67$	—	35
				$Ag_{75}In_{25}$	11.9		4000/3.6	
				$Ag_{66}In_{34}$	12.1		4600/5.8	
Ag-Sn	bilayered coatings	AlterLD	ε (0.6–6.5 eV)l	Sn/Ag	4.2	ε' < 0 (hν = 0.5–6.5 eV)	n.a.	66
				Ag/Sn	6.3		n.a.	
Ag-Sb	TF	CD-TCE	ε (0.6–6.5 eV)	Ag_xSb_{1-x} (x = 0–1)	—	n.a.	—	65
				Ag_{83}:Sb_{17}	9.7		n.a.	
				Ag_6:Sb_{94}	6.78		n.a.	
Au-Zn	B	DS	R, ε (1–7 eV)	AuZn	n.a.	n.a.	n.a.	99
Au-Cd	B	DS	R, ε (1–7 eV)	AuCd	n.a.	n.a.	n.a.	99
Au-Al	B	DS	R, ε (1.0–10.3 eV)	$AuAl_2$	n.a.	6.7 eV	~1850/1.9	102
Au-Ga	B	DS	R, ε (1.0–10.3 eV)	$AuGa_2$	n.a.	7.3 eV	~1260/4.0	102
Au-In	B	DS	R, ε (1.0–10.3 eV)	$AuIn_2$	n.a.	7.2 eV	~1336/3.65	102
	TF	CD-TCE	ε (0.6–6.5 eV)	Au_xIn_{1-x} (x = 0–1)	—	ε' < 0 (hν = 2–6.5 eV)	—	67
				Au_{85}:In_{15}	15.1		n.a.	
				Au_{25}:In_{75}	8.24		n.a.	
				Au_2:In_{98}	5.29		n.a.	

[a]DS, direct synthesis; CD, codeposition (CD-DCMS codeposition by DC magnetron sputtering; CD-TCE codeposition by thermal coevaporation); AlterLD, alternating layers' deposition; ID, interdiffusion; and hν, spectral range.

where $\varepsilon(\hbar\omega)$ and ε_m are the complex permittivities of the nanoparticles and the surrounding media, respectively.

In order to evaluate the efficiency of nanoparticles in the case of intermetallic compounds, we used published data for the complex permittivity[35,65] for calculation of the spectra of the cross-section of excitation of spherical intermetallic nanoparticles with diameter, d_{NP} = 20 nm, embedded in a dielectric medium with a refractive index of 1.5 using a procedure proposed by Cortés-López et al.[76]

With the use of the calculated optical constants of thin films, it was shown that the compositions close to the crystalline compounds in the Ag-In system, Ag_3In, Ag_9In_4, and $AgIn_2$, have lower values of σ_{ext}, and the maximum is shifted in the UV spectral area.[35] A comparison of the cross-section of extinction

σ_{ext} for intermetallic compounds containing silver and p-block metals from the Ag-Ga and Ag-In systems and those of silver and indium is presented in Figure 4a. The values of σ_{ext} were calculated using the published data.[35,77] All of them show a maximum between 3.56 and 5.75 eV. It can be seen that although the values of the maximum of σ_{ext} are smaller than that of silver, they are 1.5–2 times larger than that of indium, which has been considered as an effective material for LSPR in the UV spectral region.

The influence of the presence of an ordered phase was discussed in the case of thin Ag–In films with an island structure, and it was stated that the individual islands of the thin film can be viewed as nanoparticles on the substrate.[65] It was found that the highest enhancement of UV fluorescence of

Table 6. Synthesis Methods, Size, and Optical Properties of Nanoparticles from Intermetallic Alloys of Silver or Gold with p-Block Metals

composition	method of preparation	size	optical properties	ref
6Cd/6Ag clusters (with Ag_5Cd_8 phase)	ion implantation	$D < 20$ nm	superposition of two peaks, at 310 nm (Ag_5Cd_8) and at 412 nm (Ag)	74, 105, and 106
Au_3Zn, Au_5Zn_3, AuZn, Cu_5Zn_8-type -(Au,Zn)	one-pot reaction−thermal decomposition of precursors in hot organoamine solvent	$D < 50$ nm	absorption maximum: Au_3Zn at 495 nm Au_5Zn_3 at 485 nm	84
Ag-Al, Ag-Ga, Au-Ga, $AuGa_2$, AuGa, and Au_7Ga_2	amalgamation seeded growth−reaction between monometallic seed NCs (Au, Ag, Cu, Pd, or Ni) and amides of a second, low−melting point metal (Ga, In)		n.a.	85
Au_xGe_{1-x}	template-assisted alloying	nanowires ($D \sim 30–50$ nm $\times$ $L \sim 28$ μm)	n.a.	130
Ag_3In	SMAD method	$\sim 2–16$ nm	plasmon band, centered at 420 nm	87
$Ag_{50}In_{50}$	laser ablation	$\sim 4–5$ nm		86
$AuIn_2$	SMAD method	$\sim 2–13$ nm	absorption maximum at 520 nm	87
Au-Sn	laser dewetting of thin Ag-Sn films	35–55 nm 125–155 nm	wide band of the extinction coefficient in spectral regions from 0.5 to 4.5 eV	127
Ag_3Sn	chemical reduction of $AgNO_3$ and $SnCl_2$	~ 20 nm	two regions for LSPR excitation, ~ 1 eV and 2.3–4.0 eV	129
Ag-Bi	femtosecond laser irradiation of a $Ag_2WO_4/NaBiO_3$ target	10–15 nm	n.a.	130 and 131

tryptophane was observed in the case of thin film with composition close to the Ag_9In_4 phase.

Figure 4b presents a comparison of σ_{ext} for gold and its intermetallic crystalline phases $AuAl_2$, $AuIn_2$, and $AuGa_2$, as published data[101,102] was used for the calculations. It can be seen that the crystalline compounds $AuIn_2$ and $AuGa_2$ show a maximum in the UV spectral region at 3.66 and 4.02 eV, respectively, and significantly higher values than those of Au. The optical properties of alloys with higher p-block metal content are less well studied. The calculated optical parameters were used to determine the spectral position and the value of the maximum in σ_{ext} for nanoparticles of the same composition.[35] The obtained results suggest that such structures would have 2 times lower efficiency than similar ones with compositions close to the intermetallic compounds of silver and indium. Better efficiency can be expected at small doping of the p-block element with a noble metal, in the range of 2−5 at %, as demonstrated in the case of thin films with an island structure and composition Ag_2Sb_{98}.[65]

Reference data about the optical and plasmonic properties of Ag(Au)-p-block intermetallic compounds is summarized in Table 5. It is seen that the investigated alloys, which compositions fall in the region of intermetallic compounds of the phase diagrams, are characterized with higher plasmonic frequencies than those of solid solutions.

The results presented in this section show that the nanoparticles of intermetallic crystalline compounds of silver and gold with p-block metals can be an effective material for excitation of LSPR in the UV spectral region. For this, in the next part, we will focus on the properties of intermetallic nanoparticles.

7. NANOPARTICLES FROM NOBLE−P-BLOCK METALS

The metallic nanoparticles are potential materials for applications in catalysis, electronics, optoelectronics, information storage, biosensors, surface-enhanced Raman spectroscopy (SERS), and surface-enhanced luminescence (SEL). As it was stated in the introduction parts of our review, the preparation of intermetallic nanoparticles with controlled dimensions is extremely important for the tailoring of their properties.[79]

For the visible spectral region, the nanoparticles of silver and gold are the most widely used. The analysis of silver and gold nanoparticle nanoantenna shows maximum enhancement (expressed as a ratio between the induced electric field of the metal particle, E, and the electric field intensity of the laser radiation, E_0) and optimal wavelengths as follows: $|E|^4/|E_0|^4$ for Au dimers is 2.8×10^{11} (at 723 nm) and for Ag dimers is 1.3×10^{12} (at 794 nm).[114] It is possible to obtain an optimal tuning of the spectral position of the LSPR excitation by varying their composition and, accordingly, a variation of the fluorescence wavelength.[115,116] The fluorescence variation of Au-Ag, AuCu, and $AuCu_3$ nanoparticles is the reason why they are widely applied for detection in biosensors.[117,118]

The searching for nanoparticles (NPs) that enable excitation of LSPR in the UV is the reason for investigation of various transition metals. The analysis of nanoparticles with different shapes from the transition metals (Pt, Pd, Cr, Ni, Co, and Fe), as well as their alloys such as Pd-Ag, show that they are effective materials for excitation of LPSR in a wide interval from the UV to the near-infrared spectral regions (300−900 nm).[119−121] The best UV-SERS enhancement of Pd SSV

structure (an enhancement factor of 150) is observed in the case of NPs with 200 nm diameter.[119]

The optical characteristics of the p-block metals make them an effective material for the excitation of LSPR. Data on the synthesis of Al, Ga, and In nanoparticles can be found in the literature.[25,26,122−124] The absorption spectra of nanoparticles of these metals show that, depending on the size and shape, LSPR is observed in a wide spectral interval as follows: Al Np's (0.5−4 eV),[25,123,124] Ga NP's (1.77−5.95 eV),[26] and In NP's (2.2−6.2 eV).[123,125] The enhancing of the local electromagnetic field intensity as a result of LSPR is a phenomenon that is the basis of SERS.[126] This is the reason that nanoparticles of these p-block metals are attractive materials for the development of SERS substrates for chemical detection in the visible and UV spectral regions.[123,125] It was determined by Yang et al.[26] for dimers in vacuum with a 1 nm gap of Al and In, despite the lower values of surface-enhanced Raman spectroscopy enhancement factors, the peak values of the ratio $|E|^4/|E_0|^4$ are 2.0×10^9 (at 204 nm) for Al and 1.2×10^9 (at 359 nm) for In. Kumamoto et al.[125] have found that the Raman scattering signal of the adenine deposited on the indium-coated substrates was up to 11-times higher than that of a bare-fused silica glass substrate.

A review of the results for silver nanoparticles and p-block metals shows that LSPR, which appears as a band in the absorption spectra is observed at higher photon energies (shorter wavelengths) compared to silver nanoparticles. In the case of gold/p-block metals nanoparticles, this effect is less pronounced.

Below we will focus on the absorption data of this group of nanoparticles. Information about their composition, method of preparation, size, and optical absorption is presented in Table 6.

Silver and gold nanoparticles with the group 12 elements (Zn and Cd) at different contents of the coupled metals are presented in several works.[74,84,105,106] For the optical properties of NPs containing Ag_5Cd_8, according to the authors, a peak is observed in the absorption spectrum of 6Cd/6Ag clusters, which is a superposition of two peaks of 310 nm due to the formation of Ag_5Cd_8 and at 412 nm to elemental silver.[74] At a wavelength of 596 nm, the 6Cd/6Ag nanoparticles show larger nonlinear refractive indexes and smaller nonlinear absorption values compared to the silver nanoparticles.

The synthesis of nanoparticles from different intermetallic compounds of gold and zinc, such as Au_3Zn, Au_5Zn_3, AuZn, and Cu_5Zn_8-type-(AuZn), and their optical absorption were summarized by Schaefer et al.[84] The comparison of absorption positions shows that the Au nanoparticles absorb at 535 nm, as expected. Au_3Zn is blue-shifted relative to Au, absorbing at 495 nm. An increase in zinc content leads to a greater shift toward the shorter wavelengths, and in the case of Au_5Zn_3, the absorption maximum is at 485 nm. AuZn nanoparticles appear black and have nearly flat UV−Vis spectra, which suggest that the maximum of absorbance is shifted in the UV spectral range.

The $Ag_{50}In_{50}$ NPs, prepared by laser ablation, show an absorption maximum between that of silver and indium.[86] The synthesis of nanoparticles from the intermetallic phases containing indium, Ag_3In and $AuIn_2$ from Ag, Au, and In colloids was demonstrated in the work of Arora et al.[87] The absorption spectra show an absorption band at longer wavelengths compared to Ag/Cd nanoparticles. The absorption spectrum of $AuIn_2$ nanoparticles shows evolution of a

single band at 490 nm that is blue-shifted in comparison to the Au SPR band concomitant with a color change of the colloid from reddish brown to reddish orange.

Silver or gold nanoparticles with with Sn and Sb are also presented.[88,89,127−129] Magruder III et al.[128] applied laser dewetting of the Au−Sn film to synthesize Au−Sn NPs. Depending on the thickness of the coatings and the energy of the laser pulses, particles with sizes in the range of 30−155 nm are observed. The as-prepared nanoparticle thin films show a wide band of extinction coefficients from the IR to UV spectral regions (0.5−4.5 eV), and the position of the maximum of this band shifts from 1.6 to 2.4 eV with decreasing the thickness of the coating. The extinction coefficient values decrease at photon energies greater than 5 eV, suggesting a better efficiency for LSPR excitation. Ag/Sb clusters with different ratios of 9:3, 6:6, and 3:9, obtained by sequential implantation of Ag and Sb in silica, is reported.[128] The changes in the composition result in significantly different optical responses. An increase of the antimony content in the Ag−Sb colloid leads to a shift of the absorption maximum to shorter wavelengths.[128]

Possibilities for preparation of nanoparticles from the Ag-Bi and Au-Ge systems are proposed.[130−132] Ruiz-Ruiz et al.[130] have succeeded to prepare NPs of the silver-based solid solution in the Ag-Bi system, with a Bi content up to 5 at %. Phase separation in the Au-Ge system was used to structure nanowires with different conductivities.[132]

As a narrow band gap semiconductor Ag_2Te is suitable for preparation of quantum dots (QDs). The emission of Ag_2Te QDs, synthesized via trialkylphosphine-controlled growth, was precisely tuned in a wide range from 950 to 2100 nm.[133]

As was pointed out in general in the "Preparation" section (section 4) of our review, due to the metallic character of the intermetallic nanoparticles, an oxidation of their surface can be observed, which leads to a shift and decrease in the intensity of the LSPR band.[86] In the work of Li and Sun,[134] it was shown that under specific preparation conditions in the cases of Pt-, Pd-, and Au-based NPs, the d orbitals of transition metal atoms can interact strongly, forming an ordered structure in which the metal components are better stabilized against chemical oxidation and etching, which allows them to show a higher enhanced catalysis for electrochemical reactions, including oxygen reduction reaction (ORR), hydrogen evolution reaction (HER), formic acid oxidation reaction (FAOR), and thermooxidation reaction of CO.

8. CONCLUSIONS

A review on the preparation and optical properties of bimetallic alloys and compounds based on silver and gold with p-block metals from the Periodic table of chemical elements is proposed. Together with the boundary solid solutions, already reported as perspective for plasmonic applications due to the fluent tuning of the plasma frequency, the phase diagrams of the different bimetallic Ag(Au), p-block systems show two additional groups of promising materials, intermetallic compounds, exhibiting new properties, and continuous rows of inhomogeneous binary alloys, representing a mixture of both materials used.

The phase transitions in the compositional ranges of the systems suggest an intermittent change in the properties of Ag(Au)−p-block alloys, as the intermediate compounds may exhibit completely new values. Thus, their properties are difficult for prediction, and the experimental evaluations provide more reliable information.

The existing literature data about the plasmonic activity in the Ag(Au)−p-block intermetallic systems are extremely scant and fragmented. However, it can be seen that the addition of p-block elements, such as Zn, Cd, Al, and In, reduces the energy gap for interband transitions, associated with Ag-4d and Au-5d electronic states. As a result, the value of the imaginary part of the complex permittivity is reduced in the ultraviolet spectral range and increases the efficiency of the localized surface plasmon resonance in this region. This is seen for the structurally homogeneous phases in the systems, as solid solutions and intermediate compounds.

The Ag(Au)−p-block intermetallic compounds contain higher quantities of p-block metal and offer a well-ordered crystalline structure together with a good conductivity level, but heretofore, their optical properties have been less investigated. On the basis of the existing conductivity data, they show a reduced value of the damping parameter in the Drude dispersion model, which implies higher efficiency of LSPR compared to the strongly doped solid solutions of the noble metals. The lack of data on the complex permittivity function for a number of intermetallic compounds from Ag(Au)−p-block systems is the reason why it is not possible to trace out the changes in their plasmonic activity. However, their easy preparation and reliable plasmonic efficiency give grounds for assessment of these intermetallics as potential promising materials for UV plasmonics and further studies on their preparation as nanostructures with controlled geometry should be of particular interest.

■ AUTHOR INFORMATION

Corresponding Author

Temenuga Hristova-Vasileva − *Institute of Optical Materials and Technologies "Acad. J. Malinowski", Bulgarian Academy of Sciences, 1113 Sofia, Bulgaria; Institute of Solid State Physics, Bulgarian Academy of Sciences, 1784 Sofia, Bulgaria;* ◉ orcid.org/0000-0002-0929-5277; Email: teddie@issp.bas.bg

Authors

Rosen Todorov − *Institute of Optical Materials and Technologies "Acad. J. Malinowski", Bulgarian Academy of Sciences, 1113 Sofia, Bulgaria;* ◉ orcid.org/0000-0002-7674-1476

Vesela Katrova − *Institute of Optical Materials and Technologies "Acad. J. Malinowski", Bulgarian Academy of Sciences, 1113 Sofia, Bulgaria*

Anna Atanasova − *Institute of Optical Materials and Technologies "Acad. J. Malinowski", Bulgarian Academy of Sciences, 1113 Sofia, Bulgaria*

Complete contact information is available at:
https://pubs.acs.org/10.1021/acsomega.2c05943

Notes

The authors declare no competing financial interest.

■ REFERENCES

(1) Zayats, A. V.; Smolyaninov, I. I.; Maradudin, A. A. Nano-optics of surface plasmon polaritons. *Phys. Rep.* **2005**, *408*, 131−314.

(2) Ekgasit, S.; Thammacharoen, C.; Yu, F.; Knoll, W. Evanescent field in surface plasmon resonance and surface plasmon field-enhanced fluorescence spectroscopies. *Anal. Chem.* **2004**, *76*, 2210−2219.

(3) Qu, J.-H.; Dillen, A.; Saeys, W.; Lammertyn, J.; Spasic, D. Advancements in SPR biosensing technology: An overview of recent trends in smart layers design, multiplexing concepts, continuous monitoring and in vivo sensing. *Anal. Chim. Acta* **2020**, *1104*, 10−27.

(4) Andrade, G. F. S.; Brolo, A. G. Nanoplasmonic Structures in Optical Fibers. In *Nanoplasmonic Sensors. Integrated Analytical Systems*; Dmitriev, A., Ed.; Springer: New York, NY, 2012; pp 289−315.

(5) Tan, H.; Sivec, L.; Yan, B.; Santbergen, R.; Zeman, M.; Smets, A. H. M. Improved light trapping in microcrystalline silicon solar cells by plasmonic back reflector with broad angular scattering and low parasitic absorption. *Appl. Phys. Lett.* **2013**, *102*, 153902.

(6) Huang, J. A.; Mousavi, M. Z.; Zhao, Y.; Hubarevich, A.; Omeis, F.; Giovannini, G.; Schütte, M.; Garoli, D.; De Angelis, F. SERS discrimination of single DNA bases in single oligonucleotides by electro-plasmonic trapping. *Nat. Commun.* **2019**, *10*, 5321.

(7) Xu, D.-D.; Zheng, B.; Song, C.-Y.; Lin, Y.; Pang, D.-W.; Tang, H.-W. Metal-enhanced fluorescence of gold nanoclusters as a sensing platform for multi-component detection. *Sens. Actuators B Chem.* **2019**, *282*, 650−658.

(8) Cortes, C. L.; Newman, W.; Molesky, S.; Jacob, Z. Quantum nanophotonics using hyperbolic metamaterials. *J. Opt.* **2012**, *14*, 063001.

(9) Shabani, A.; Tsegay Korsa, M.; Petersen, S.; Khazaei Nezhad, M.; Kumar Mishra, Y.; Adam, J. Zirconium nitride: optical properties of an emerging intermetallic for plasmonic applications. *Adv. Photonics Res.* **2021**, *2*, 2100178.

(10) Ni, J. H.; Sarney, W. L.; Leff, A. C.; Cahill, J. P.; Zhou, W. Property variation in wavelength thick epsilon-near-zero ITO metafilm for near IR photonic devices. *Sci. Rep.* **2020**, *10*, 713.

(11) Zhao, D.; Lin, Z.; Zhu, W.; Lezec, H. J.; Xu, T.; Agrawal, A.; Zhang, C.; Huang, K. Recent advances in ultraviolet nanophotonics: from plasmonics and metamaterials to metasurfaces. *Nanophotonics.* **2021**, *10*, 2283−2308.

(12) Ghori, M. Z.; Veziroglu, S.; Hinz, A.; Shurtleff, B. B.; Polonskyi, O.; Strunskus, T.; Adam, J.; Faupel, F.; Aktas, O. C. Role of UV plasmonics in the photocatalytic performance of TiO_2 decorated with aluminum nanoparticles. *ACS Appl. Nano Mater.* **2018**, *1*, 3760−3764.

(13) McMahon, J. M.; Gray, S. K.; Schatz, G. C. Ultraviolet plasmonics: The poor metals Al, Ga, In, Sn, Tl, Pb, and Bi. *Phys. Chem. Chem. Phys.* **2013**, *15*, 5415−5423.

(14) Gutierrez, Y.; Ortiz, D.; Saiz, J.; Gonzalez, F.; Moreno, F. Plasmonics in the ultraviolet with aluminum, gallium, magnesium and rhodium. *Appl. Sci.* **2018**, *8*, 64.

(15) Gong, C.; Leite, M. S. Noble metal alloys for plasmonics. *ACS Photonics* **2016**, *3* (4), 507−513.

(16) Simmons, J.; Potter, K. *Optical Materials*; Academic Press, 2000.

(17) Ehrenreich, H.; Philipp, H. R. Optical properties of Ag and Cu. *Phys. Rev.* **1962**, *128*, 1622−1629.

(18) Peña-Rodríguez, O.; Caro, M.; Rivera, A.; Olivares, J.; Perlado, J. M.; Caro, A. Optical properties of Au-Ag alloys: An ellipsometric study. *Opt. Mater. Express* **2014**, *4*, 403−410.

(19) Peña-Rodríguez, O. Modelling the dielectric function of Au-Ag alloys. *J. Alloys Compd.* **2017**, *694*, 857−863.

(20) Blaber, M. G.; Arnold, M. D.; Ford, M. J. Designing materials for plasmonic systems: the alkali-noble intermetallics. *J. Phys.: Condens. Matter* **2010**, *22*, 095501.

(21) Zamora Zeledon, J. A.; Stevens, M. B.; Gunasooriya, G. T. K. K.; Gallo, A.; Landers, A. T.; Kreider, M. E.; Hahn, C.; Nørskov, J. K.; Jaramillo, T. F. Tuning the electronic structure of Ag-Pd alloys to enhance performance for alkaline oxygen reduction. *Nat. Commun.* **2021**, *12*, 620.

(22) Luong, H. M.; Pham, M. T.; Ai, B.; Nguyen, T. D.; Zhao, Y. Magnetoplasmonic properties of Ag-Co composite nanohole arrays. *Phys. Rev. B* **2019**, *99*, 224413.

(23) Luong, H. M.; Pham, M. T.; Nguyen, T. D.; Zhao, Y. Magneto-plasmonic properties of Ag-Co composite nano-triangle arrays. *Nanotechnology* **2019**, *30*, 425203.

(24) Shklyarevskii, I. N.; Bondarenko, Yu.Yu.; Makarovskii, N. A. Plasma resonance in granular gallium films deposited on rough NACl and KCl single-crystal surfaces. *Opt. Spectrosc.* **2000**, *88*, 547−550.

(25) Ross, M. B.; Schatz, G. C. Aluminum and indium plasmonic nanoantennas in the ultraviolet. *J. Phys. Chem. C* **2014**, *118*, 12506−12514.

(26) Yang, Y.; Akozbek, N.; Kim, T.-H.; Sanz, J. M.; Moreno, F.; Losurdo, M.; Brown, A. S.; Everitt, H. O. Ultraviolet-visible plasmonic properties of gallium nanoparticles investigated by variable-angle spectroscopic and mueller matrix ellipsometry. *ACS Photonics* **2014**, *1*, 582−589.

(27) Koyama, R. Y.; Smith, N. V.; Spicer, W. E. Optical Properties of Indium. *Phys. Rev. B* **1973**, *8*, 2426−2432.

(28) Lenham, A. P.; Treherne, M.; Metcalfe, R. J. Optical properties of antimony and bismuth crystals. *J. Opt. Soc. Am.* **1965**, *55*, 1072−1074.

(29) Rerek, T.; Skowronski, L.; Szczesny, R.; Naparty, M.K.; Derkowska-Zielinska, B. The effect of the deposition rate on microstructural and opto-electronic properties of β-Sn layers. *Thin Solid Films* **2019**, *670*, 86−92.

(30) Lindquist, N. C.; Nagpal, P.; McPeak, K. M.; Norris, D. J.; Oh, S. Engineering metallic nanostructures for plasmonics and nano-photonics. *Rep. Prog. Phys.* **2012**, *75*, 036501.

(31) Blaber, M. G.; Arnold, M. D.; Ford, M. J. A review of the optical properties of alloys and intermetallics for plasmonics. *J. Phys.: Condens. Matter* **2010**, *22*, 143201.

(32) *Handbook of Optical Constants of Solids III*; Palik, E. D., Ed.; Academic Press, 1998.

(33) Jezequel, G.; Lemonnier, J. C.; Thomas, J. Optical properties of gallium films between 2 and 15 eV. *J. Phys. F: Metal Phys.* **1977**, *7*, 1613.

(34) Bor, J.; Bartholomew, C. The optical properties of indium, gallium and thallium. *Proc. Phys. Soc.* **1967**, *90*, 1153.

(35) Todorov, R.; Hristova-Vasileva, T.; Katrova, V.; Atanasova, A.; Milushev, G. Electronic structure and plasmonic activity in co-evaporated Ag-In bimetallic alloys. *J. Alloys Compd.* **2022**, *897*, 163253.

(36) Tediosi, R.; Armitage, N. P.; Giannini, E.; van der Marel, D. Charge Carrier Interaction with a Purely Electronic Collective Mode: Plasmarons and the Infrared Response of Elemental Bismuth. *Phys. Rev. Lett.* **2007**, *99*, 016406.

(37) *Intermetallic chemistry*; Ferro, R.; Saccone, A., Eds.; Pergamon Materials Series, 2007; Vol. 13.

(38) De Haas, W. J.; Jurriaanse, F. Die supraleitfähigkeit des gold-wismuts. *Sci. Nat.* **1931**, *19*, 706.

(39) Cheng, S.; Huang, C.-M.; Pecht, M. A review of lead-free solders for electronics applications. *Microelectron. Reliab.* **2017**, *75*, 77−95.

(40) Hansen, M.; Anderko, K. *Constitution of Binary Alloys, Metallurgy and Metallurgical Engineering Series*; McGraw and Hill Book Company Inc.: New York, 1958.

(41) Massalski, T. B.; Mizutani, U. Electronic structure of Hume-Rothery phases. *Prog. Mater. Sci.* **1978**, *22*, 151−262.

(42) Okamoto, H.; Massalski, T. B. The Au-Pb (Gold-Lead) system. *Bull. Alloy Phase Diagr.* **1984**, *5*, 276−284.

(43) Froes, F. H.; Suryanarayana, C.; Russell, K.; Li, C.-G. Synthesis of intermetallics by mechanical alloying. *Mater. Sci. Eng., A* **1995**, *192−193*, 612−623.

(44) Puttlitz, K. J.; Stalter, K. A. *Handbook of Lead-Free Solder Technology for Microelectronic Assemblies; G. Interface reactions with Gold, Silver and Palladium*; CRC Press, 2004.

(45) Bystrom, A.; Almin, K. E.; Sillen, L. G.; Linnasalmi, A.; Laukkanen, P. X-ray investigation of gold-cadmium alloys rich in gold. *Acta Chem. Scand.* **1947**, *1*, 76−89.

(46) Massalski, T. B. The lattice spacings of close-packed hexagonal Au-In, Au-Cd, and Au-Hg alloys. *Acta Metall.* **1957**, *5*, 541−547.

(47) Puselj, M.; Schubert, K. Kristallstrukturen von $Au_9In_4(h)$ und Au_7In_3. *J. Less-common. Met.* **1975**, *41*, 33−44.

(48) Jandali, M. Z.; Rajasekharan, T.; Shchubert, K. Crystal structure of $Au_{10}In_3$. *Z. Metallkd.* **1982**, *73*, 463−467.

(49) Cabri, L. J. P. Discussion of "Empressite and stuetzite redefined" by R. M. Honea. *Am. Mineral.* **1965**, *50*, 795−801.

(50) Imamov, R. M.; Pinsker, Z. G. Determination of the crystal structure of the hexagonal phase in the silver-tellurium system. *Sov. Phys. Crystallogr.* **1966**, *11*, 182−188.

(51) Ellner, M. Über kristallchemische Parameter metastabiler intermetallischer Verbindungen. *Z. Met.kd.* **1985**, *76*, 372−377.

(52) Ellner, M.; Predel, B. Zur metastabilen Phase Au4Si*m. *Z. Met.kd.* **1980**, *71*, 364−369.

(53) Che, G.-C.; Liang, J.-K.; Jin, Z.-W.; Zhao, Z.-X. A study on phase relations of rapidly quenched alloys in the Ag-Ge systems. *Acta. Phys. Sin.* **1985**, *34*, 476−483.

(54) Anantharaman, T. R.; Luo, H. L.; Klement, W. Nonequilibrium structures in gold-germanium alloys. *Trans TMS-AIME* **1965**, *233*, 2014−2017.

(55) Anantharaman, T. R.; Luo, H. L.; Element, W. Formation of new intermetallic phases in binary eutectic systems by drastic undercooling of the melt. *Nature* **1966**, *210*, 1040−1041.

(56) Schluckebier, G.; Predel, B. Untersuchung zur Struktur metastabiler Phasen im System Gold-Germanium. *Z. Met.kd.* **1980**, *71*, 535−541.

(57) Kim, K. J.; Chen, L.-Y.; Lynch, D. W. Ellipsometric study of optical transitions in $Ag_{1-x}In_x$ alloys. *Phys. Rev. B* **1988**, *38*, 13107−13112.

(58) Taher, M.; Mao, F.; Berastegui, P.; Andersson, A. M.; Jansson, U. Tuning tribological, mechanical and electrical properties of Ag-X (X = Al, In, Sn) alloys. *Tribol. Int.* **2018**, *125*, 121−127.

(59) Shiraishi, T.; Hisatsune, K.; Tanaka, Y.; Miura, E.; Takuma, Y. Optical properties of Au-Pt and Au-Pt-In alloys. *Gold Bull.* **2001**, *34*, 129−133.

(60) Kamal, M.; El-Bediwi, A. B.; El-Ashram, T.; Dorgham, M. E. The role of valence electron concentration on the structure and properties of rapidly solidified Sn-Ag binary alloys. *Mater. Sci. Appl.* **2012**, *03*, 179−184.

(61) Horo, J.; Harne, P. G.; Nayak, B. B.; Vitta, S. Low temperature coefficient of resistivity Ag-Cd and Ag-Sn alloys—structure and transport. *Mater. Sci. Eng., B* **2004**, *107*, 53−57.

(62) Nishimura, K.; Kakihana, M.; Nakamura, A.; Aoki, D.; Harima, H.; Hedo, M.; Nakama, T.; Ōnuki, Y. Fermi surfaces of the pyrite-type cubic $AuSb_2$ compared with split Fermi surfaces of the ullmannite-type cubic chiral NiSbS and PdBiSe. *Phys. B: Condens. Matter* **2018**, *536*, 643−648.

(63) Yeh, T.-T.; Lin, W. H.; Tzeng, W.-Y.; Le, P. H.; Luo, C.-W.; Milenov, T. I. The optical properties of Ag_2Te crystals from THz to UV. *J. Alloys Compd.* **2017**, *725*, 433−440.

(64) Hsu, L.-S.; Guo, R. G. Y.; Denlinger, R. J. D.; Allen, J. W. Experimental and theoretical studies of the electronic structures of $AuAl_2$ and $PtGa_2$. *Surf. Rev. Lett.* **2002**, *09*, 1251−1255.

(65) Katrova, V.; Hristova-Vasileva, T.; Atanasova, A.; Strijkova, V.; Todorov, R. Optical properties of nanostructured bimetallic films from the Ag-In and Ag-Sb systems and their surface enhanced fluorescence application. *J. Phys.: Conf. Ser.* **2022**, *2240*, 012007.

(66) Wronkowska, A. A.; Wronkowski, A.; Kuklinski, K.; Senski, M.; Skowronski, Ł. Spectroscopic ellipsometry study of the dielectric response of Au-In and Ag-Sn thin-film couples. *Appl. Surf. Sci.* **2010**, *256*, 4839−4844.

(67) Todorov, R.; Hristova-Vasileva, T.; Atanasova, A.; Katrova, V.; Milushev, G. Preparation and optical characterization of Au - In films for plasmonic applications. *J. Phys.: Conf. Ser.* **2021**, *1762*, 012022.

(68) Todorov, R.; Hristova-Vasileva, T.; Atanasova, A.; Katrova, V. Thin Ag/Bi coatings as epsilon-near-zero material with low optical losses. *Opt. Mater.* **2022**, *124*, 112040.

(69) Chen, L.-Y. *Optical properties of metals and alloys: Au, Ag, FeRh, $AuAl_2$, and $PtAl_2$*. Ph.D. Dissertation, Iowa State University, 1987, DOI: 10.31274/RTD-180813-12939.

(70) Nedyalkov, N.; Nikov, R.; Dikovska, A.; Atanasova, G.; Nakajima, Y.; Terakawa, M. Gold nanostructures deposition by laser ablation in air using nano- and femtosecond laser pulses. *Appl. Phys. A-Mater.* **2017**, *123*, 306.

(71) Auer, S.; Wan, W.; Huang, X.; Ramirez, A. G.; Cao, H. Morphology-induced plasmonic resonances in silver-aluminum alloy thin films. *Appl. Phys. Lett.* **2011**, *99*, 041116.

(72) Yang, G.; Sun, J.; Zhou, J. Dielectric properties of aluminum silver alloy thin films in optical frequency range. *J. Appl. Phys.* **2011**, *109*, 123105.

(73) Fang, Y. H.; Kuo, P. C.; Chen, P. W.; Hsu, W.-C.; Chou, C. Y.; Wu, T. H. Optical properties of inorganic AgSb recording thin film. *Appl. Phys. Lett.* **2006**, *88*, 261917.

(74) Zuhr, R. A.; Magruder, R. H.; Anderson, T. S. Formation and optical properties of intermetallic nanoclusters formed by sequential ion implantation. *Surf. Coat. Technol.* **1998**, *103*−*104*, 401−408.

(75) Todorov, R.; Hristova-Vasileva, T.; Atanasova, A.; Katrova, V.; Strijkova, V.; Milushev, G.; Milanov, E. Optical properties of thin Ag-In films prepared by interdiffusion in bimetallic nanolayered stacks. *J. Phys.: Conf. Ser.* **2021**, *1762*, 012023.

(76) Cortés-López, S.; Gastélum-Acuña, S. L.; Flores-Ruiz, F. J.; Garcia-Vazquez, V.; García-Llamas, R.; Pérez-Rodríguez, F. Berreman effect in bimetallic nanolayered metamaterials. *Opt. Mater.* **2020**, *99*, 109578.

(77) Lereu, A. L.; Lemarchand, F.; Zerrad, M.; Yazdanpanah, M.; Passian, A. Optical properties and plasmonic response of silver-gallium nanostructures. *J. Appl. Phys.* **2015**, *117*, 063110.

(78) Green, E. L.; Muldawer, L. Optical properties of the alpha-phase alloys Ag-Zn and Ag-Cd. *Phys. Rev. B* **1970**, *2*, 330−340.

(79) Srinoi, P.; Chen, Y.-T.; Vittur, V.; Marquez, M.; Lee, T. Bimetallic nanoparticles: Enhanced magnetic and optical properties for emerging biological applications. *Appl. Sci.* **2018**, *8*, 1106.

(80) Zhou, M.; Li, C.; Fang, J. Noble-metal based random alloy and intermetallic nanocrystals: Syntheses and applications. *Chem. Rev.* **2021**, *121*, 736−795.

(81) Cortie, M. B.; McDonagh, A. M. Synthesis and optical properties of hybrid and alloy plasmonic nanoparticles. *Chem. Rev.* **2011**, *111*, 3713−3735.

(82) Loza, K.; Heggen, M.; Epple, M. Synthesis, structure, properties, and applications of bimetallic nanoparticles of noble metals. *Adv. Funct. Mater.* **2020**, *30*, 1909260.

(83) Cable, R. E.; Schaak, R. E. Low-temperature solution synthesis of nanocrystalline binary intermetallic compounds using the polyol process. *Chem. Mater.* **2005**, *17*, 6835−6841.

(84) Schaefer, Z. L.; Vaughn, D. D.; Schaak, R. E. Solution chemistry synthesis, morphology studies, and optical properties of five distinct nanocrystalline Au-Zn intermetallic compounds. *J. Alloys Compd.* **2010**, *490*, 98−102.

(85) Clarysse, J.; Moser, A.; Yarema, O.; Wood, V.; Yarema, M. Size- and composition-controlled intermetallic nanocrystals via amalgamation seeded growth. *Sci. Adv.* **2021**, *7*, No. 1.

(86) Cottancin, E.; Langlois, C.; Lerme, J.; Broyer, M.; Lebeault, M.-A.; Pellarin, M. Plasmon spectroscopy of small indium-silver clusters: monitoring the indium shell oxidation. *Phys. Chem. Chem. Phys.* **2014**, *16*, 5763−5773.

(87) Arora, N.; Jagirdar, B. R.; Klabunde, K. J. Digestive ripening facilitated atomic diffusion at nanosize regime: Case of $AuIn_2$ and Ag_3In intermetallic nanoparticles. *J. Alloys Compd.* **2014**, *610*, 35−44.

(88) Lalisse, A.; Tessier, G.; Plain, J.; Baffou, G. Quantifying the efficiency of plasmonic materials for near-field enhancement and photothermal conversion. *J. Phys. Chem. C* **2015**, *119*, 25518−25528.

(89) Toudert, J.; Serna, R. Interband transitions in semi-metals, semiconductors, and topological insulators: a new driving force for

plasmonics and nanophotonics. *Opt. Mater. Express* **2017**, *7*, 2299−2325.

(90) De Silva, K. S. B.; Keast, V. J.; Gentle, A.; Cortie, M. B. Optical properties and oxidation of α-phase Ag-Al thin films. *Nanotechnology* **2017**, *28*, 095202.

(91) Staines, M. Piezoreflectance and electronic structure of alloys of copper with polyvalent solutes. *Phys. Rev. B* **1981**, *24*, 7143−7154.

(92) Prandini, G.; Rignanese, G.-M.; Marzari, N. Photorealistic modelling of metals from first principles. *Npj Comput. Mater.* **2019**, *5*, 129.

(93) Kalas, B.; Sáfrán, G.; Serényi, M.; Fried, M.; Petrik, P. Scanning-resonance optical sensing based on a laterally graded plasmonic layer—optical properties of Ag_xAl_{1-x} in the range of x = 0 to 1. *Appl. Surf. Sci.* **2022**, *606*, 154770.

(94) Satow, T.; Uemura, O.; Yamakawa, S. X-ray diffraction and electrical resistivity study of Ag_2In and high temperature Ag_3In phases. *Trans. Jpn. Inst. Met.* **1974**, *15*, 253−255.

(95) Uemura, O.; Satow, T. Order-disorder transition of Ag_3In. *Trans. Jpn. Inst. Met.* **1973**, *14*, 199−201.

(96) Tian, Y.; Zhang, Q. M.; Li, Z. Q. Electrical transport properties of Ag_3Sn compound. *Solid State Commun.* **2011**, *151*, 1496−1499.

(97) Bridgman, P. W. Compressibilities and electrical resistance under pressure, with special reference to intermetallic compounds. *Proc. Am. Acad. Arts Sci.* **1935**, *70*, 285−317.

(98) Uemura, O.; Ikeda, S. Electrical resistivity, magnetic susceptibility, and heat of mixing of liquid silver-germanium alloys. *Trans. Jpn. Inst. Met.* **1973**, *14*, 351−354.

(99) Amar, H.; Johnson, K. H.; Wang, K. P. Electronic structure of IB-IIB Beta-phase alloys. *Phys. Rev.* **1966**, *148*, 672−680.

(100) Muldawer, L. Spectral reflectivity as a function of temperature of β-brass type alloys. *Phys. Rev.* **1962**, *127*, 1551−1559.

(101) Keast, V. J.; Birt, K.; Koch, C. T.; Supansomboon, S.; Cortie, M. B. The role of plasmons and interband transitions in the color of $AuAl_2$, $AuIn_2$, and $AuGa_2$. *Appl. Phys. Lett.* **2011**, *99*, 111908.

(102) Vishnubhatla, S. S.; Jan, J.-P. Optical properties of the intermetallic compounds $AuAl_2$, $AuGa_2$ and $AuIn_2$. *Philos. Mag.* **1967**, *16*, 45−50.

(103) Supansomboon, S. S.; Dowd, A.; van der Lingen, E.; Keast, V. J.; Cortie, M. B. Coatings of coloured intermetallic compounds for decorative and technological application. In *Materials Forum*; Howard, P., Huggett, P., Evans, D., Eds.; Institute of Materials Engineering Australasia Ltd, 2013; Vol. 37.

(104) Gupta, A.; Sen Gupta, R.; Goswami, K. Electronic and optical properties of some intermetallics. *J. Phys. (Paris)* **1994**, *4*, 1867−1876.

(105) Zuhr, R. A.; Magruder, R. H.; Anderson, T. S. Optical properties of multi-component cadmium-silver nanocluster composites formed in silica by sequential ion implantation. *Mater. Res. Soc. Symp. Proc.* **1996**, *438*, 411−416.

(106) Anderson, T. S.; Magruder, R. H., III; Kinser, D. L.; Zuhr, R. A.; Thomas, D. K. Formation and optical properties of metal nanoclusters formed by sequential implantation of Cd and Ag in silica. *Nucl. Instrum. Methods Phys. Res. B* **1997**, *124*, 40−46.

(107) Yu, C.-F.; Cheng, H-Ch.; Chen, W.-H. Structural, mechanical, thermodynamic and electronic properties of $AgIn_2$ and Ag_3In intermetallic compounds: ab initio investigation. *RSC Adv.* **2015**, *5*, 70609−70618.

(108) Kumar, S.; Jung, J. P. Mechanical and electronic properties of Ag_3Sn intermetallic compound in lead free solders using ab initio atomistic calculation. *Mater. Sci. Eng., B* **2013**, *178*, 10−21.

(109) Gnanapoongothai, T.; Murugan, R.; Palanivel, B. First-principle study on lithium intercalated antimonides Ag_3Sb and Mg_3Sb_2. *Ionics* **2015**, *21*, 1351−1361.

(110) Kashida, S.; Watanabe, N.; Hasegawa, T.; Iida, H.; Mori, M. Electronic structure of Ag_2Te, band calculation and photoelectron spectroscopy. *Solid State Ion.* **2002**, *148*, 193−201.

(111) Ahn, J.; Sellmyer, D. J. Fermi surface of $AuSb_2$. I. High-field galvanomagnetic effects. *Phys. Rev. B* **1970**, *1*, 1273−1284.

(112) Karpiński, K.; Zielińska-Raczyńska, S.; Ziemkiewicz, D. Long-range plasmons and epsilon-near-zero modes in ultraviolet. *J. Opt. Soc. Am. B* **2021**, *38*, 79−87.

(113) Novotny, L.; Hecht, B. *Surface plasmons*. In *Principles of Nano-Optics*; Cambridge University Press, Cambridge, 2012; pp 369−413.

(114) Blaber, M. G.; Schatz, G. C. Extending SERS into the infrared with gold nanosphere dimers. *Chem. Commun.* **2011**, *47*, 3769−3771.

(115) Xu, D.-D.; Zheng, B.; Song, C.-Y.; Lin, Y.; Pang, D.-W.; Tang, H.-W. Metal-enhanced fluorescence of gold nanoclusters as a sensing platform for multi-component detection. *Sens. Actuators B Chem.* **2019**, *282*, 650−658.

(116) Liu, S.; Chen, G.; Prasad, P. N.; Swihart, M. T. Synthesis of monodisperse Au, Ag, and Au-Ag alloy nanoparticles with tunable size and surface plasmon resonance frequency. *Chem. Mater.* **2011**, *23*, 4098−4101.

(117) Wang, C. I.; Chen, W.-T.; Chang, H.-T. Enzyme mimics of Au/Ag nanoparticles for fluorescent detection of acetylcholine. *Anal. Chem.* **2012**, *84*, 9706−9712.

(118) Sra, A. K.; Ewers, T. D.; Schaak, R. E. Direct solution synthesis of intermetallic AuCu and $AuCu_3$ nanocrystals and nanowire networks. *Chem. Mater.* **2005**, *17*, 758−766.

(119) Manchon, D.; Lermé, J.; Zhang, T.; Mosset, A.; Jamois, C.; Bonnet, C.; Rye, J.-M.; Belarouci, A.; Broyer, M.; Pellarin, M.; Cottancin, E. Plasmonic coupling with most of the transition metals: a new family of broad band and near infrared nanoantenna. *Nanoscale* **2015**, *7*, 1181−1192.

(120) Cui, L.; Mahajan, S.; Cole, R. M.; Soares, B.; Bartlett, P. N.; Baumberg, J. J.; Hayward, I. P.; Ren, B.; Russell, A. E.; Tian, Z. Q. UV SERS at well ordered Pd sphere segment void (SSV) nanostructures. *Phys. Chem. Chem. Phys.* **2009**, *11*, 1023−1026.

(121) Liu, S.; Li, Y.; Yu, X.; Han, S.; Zhou, Y.; Yang, Y.; Zhang, H.; Jiang, Z.; Zhu, C.; Li, W.-X.; Wöll, C.; Wang, Y.; Shen, W. Tuning crystal-phase of bimetallic single-nanoparticle for catalytic hydrogenation. *Nat. Commun.* **2022**, *13*, 4559.

(122) Martin, J.; Plain, J. Fabrication of aluminium nanostructures for plasmonics. *J. Phys. D: Appl. Phys.* **2015**, *48*, 184002.

(123) Das, R.; Soni, R. K. Synthesis and surface-enhanced Raman scattering of indium nanotriangles and nanowires. *RSC Adv.* **2017**, *7*, 32255.

(124) Langhammer, C.; Schwind, M.; Kasemo, B.; Zorić, I. Localized surface plasmon resonances in aluminum nanodisks. *Nano Lett.* **2008**, *8*, 1461−1471.

(125) Kumamoto, Y.; Taguchi, A.; Honda, M.; Watanabe, K.; Saito, Y.; Kawata, S. Indium for deep-ultraviolet surface-enhanced resonance Raman scattering. *ACS Photonics* **2014**, *1*, 598−603.

(126) Ding, S. Y.; Yi, J.; Li, J. F.; Ren, B.; Wu, D. Y.; Panneerselvam, R.; Tian, Z. Q. Nanostructure-based plasmon-enhanced Raman spectroscopy for surface analysis of materials. *Nat. Rev. Mater.* **2016**, *1*, 1−16.

(127) Dzienny, P.; Szczęsny, R.; Rerek, T.; Trzcinski, M.; Skowronski, L.; Antonczak, A. Laser-induced alloy nanoparticles on Au-Sn thin layers. *Appl. Surf. Sci.* **2022**, *591*, 153147.

(128) Magruder, R.H.; Anderson, T.S.; Zuhr, R.A.; Thomas, D.K. Formation and optical characterization of multi-component Ag-Sb nanometer dimension colloids formed by sequential ion implantation in silica. *Nucl. Instrum. Methods Phys. Res. B* **1996**, *108*, 305−312.

(129) Atanasova, A.; Katrova, V.; Hristova-Vasileva, T.; Todorov, R. Synthesis, microstructure, and optical properties of Ag_3Sn nanoparticles for plasmonic sensing applications. *Proc. SPIE* **2021**, *11919*, 1191927.

(130) Ruiz-Ruiz, V.-F.; Zumeta-Dube, I.; Diaz, D.; Arellano-Jimenez, M. J.; Jose-Yacaman, M. Can silver be alloyed with bismuth on nanoscale? An optical and structural approach. *J. Phys. Chem. C* **2017**, *121*, 940−949.

(131) Machado, T. R.; Macedo, N. G.; Assis, M.; Donate-Buendia, C.; Minguez-Vega, G.; Teixeira, M. M.; Foggi, C. C.; Vergani, C. E.; Beltran-Mir, H.; Andres, J.; Cordoncillo, E.; Longo, E. From complex inorganic oxides to Ag-Bi nanoalloy: synthesis by femtosecond laser irradiation. *ACS Omega* **2018**, *3*, 9880−9887.

(132) Chueh, Y.-L.; Boswell, C. N.; Yuan, C.-W.; Shin, S. J.; Takei, K.; Ho, J. C.; Ko, H.; Fan, Z.; Haller, E. E.; Chrzan, D. C.; Javey, A. Nanoscale structural engineering via phase segregation: Au-Ge system. *Nano Lett.* **2010**, *10*, 393−397.

(133) Liu, Z.-Y.; Liu, A.-A.; Fu, H.; Cheng, Q.-Y.; Zhang, M.-Y.; Pan, M.-M.; Liu, L.-P.; Luo, M.-Y.; Tang, B.; Zhao, W.; Kong, J.; Shao, X.; Pang, D.-W. Breaking through the size control dilemma of silver chalcogenide quantum dots via trialkylphosphine-induced ripening: leading to Ag_2Te emitting from 950 to 2100 nm. *J. Am. Chem. Soc.* **2021**, *143*, 12867−12877.

(134) Li, J.; Sun, S. Intermetallic nanoparticles: synthetic control and their enhanced electrocatalysis. *Acc. Chem. Res.* **2019**, *52*, 2015−2025.